

The 1998 March 14 Fandoqa earthquake (M_w 6.6) in Kerman province, southeast Iran: re-rupture of the 1981 Sirch earthquake fault, triggering of slip on adjacent thrusts and the active tectonics of the Gowk fault zone

M. Berberian,¹ J. A Jackson,² E. Fielding,³ B. E Parsons,⁴ K. Priestley,²
M. Qorashi,⁵ M. Talebian,^{2,5} R. Walker,² T. J Wright⁴ and C. Baker²

¹Najarian Associates, Suite E, One Industrial Way West, Eatontown, NJ 07724-2255, USA. E-mail: berberian@najarian.com

²University of Cambridge, Department of Earth Sciences, Bullard Laboratories, Madingley Road, Cambridge, CB3 0EZ, UK. E-mails: jackson@esc.cam.ac.uk; priestley@esc.cam.ac.uk

³Jet Propulsion Laboratory, California Institute of Technology, 4800 Oak Grove Drive, Pasadena, CA 91109, USA. E-mail: EricF@sierras.jpl.nasa.gov

⁴University of Oxford, Department of Earth Sciences, Parks Road, Oxford, OX1 3PR, UK E-mails: barry.parsons@earth.ox.ac.uk; tim.wright@earth.ox.ac.uk

⁵Geological Survey of Iran, PO Box 13185-1494, Tehran, Iran. E-mail: seismotec@www.dci.co.ir

Accepted 2001 March 5. Received 2001 February 20; in original form 2000 August 7

SUMMARY

The 1998 March 14 Fandoqa earthquake (M_s 6.6) was the penultimate in a series of five substantial earthquakes on the Gowk fault system of southeast Iran since 1981, all of which were associated with co-seismic surface ruptures. We use observations of surface faulting, analysis of P and SH body waves, SAR interferometry and geomorphology to investigate the ruptures in these earthquakes and how they are related both to each other and to the regional active tectonics. The 1998 Fandoqa earthquake produced 23 km of surface faulting with up to 3 m right-lateral strike-slip and 1 m vertical offsets. SAR interferometry and seismic waveforms show that the main rupture plane dipped west at $\sim 50^\circ$ and had a normal component, although the surface ruptures were more complicated, being downthrown to both the east and the west on steep faults in near-surface sediments. In addition, SAR interferometry shows that a nearby thrust with a similar strike but dipping at $\sim 6^\circ W$ moved about 8 cm in a time interval and in a position that makes it likely that its slip was triggered by the Fandoqa earthquake. The 1998 surface ruptures in the Gowk valley followed part of a much longer (~ 80 km) set of co-seismic ruptures with smaller offsets that were observed after larger earthquakes in 1981 (M_w 6.6 and 7.1). The main ruptures in these 1981 earthquakes probably occurred on different, deeper parts of the same fault system, producing only minor reactivation of the shallower faults at the surface. Although the 1981–1998 earthquake sequence apparently ruptured parts of the same fault system repeatedly, these earthquakes had very different rupture characteristics: an important lesson for the interpretation of both palaeoseismological trenching investigations and historical accounts of earthquakes. The regional kinematics, which involve oblique right-lateral and convergent motion, are evidently achieved by a complex configuration of faults with normal, reverse and strike-slip components. Some of the complexity at the surface may be related to a ramp-and-flat fault geometry at depth, but could also be related to the large topographic contrast of ~ 2000 m across the fault system, which separates the high Kerman plateau from the low Dasht-e-Lut desert. Details of the fault geometry at depth remain speculative, but it must be unstable and evolve with time. It may be this requirement that causes the principal features of geological ‘flower structures’ to develop, such as series of subparallel faults which accommodate dip-slip components of motion.

Key words: continental tectonics, earthquakes, Iran, SAR interferometry, seismology.

1 INTRODUCTION

On 14 March 1998 a destructive earthquake of M_w 6.6 occurred in the Kerman province of SE Iran. This earthquake is interesting for a number of reasons. First, it ruptured about 20 km of the Gowk fault system, a right-lateral strike-slip zone bordering the western edge of the Dasht-e-Lut desert, and produced co-seismic faulting with horizontal offsets of up to 3 m. Second, synthetic aperture radar (SAR) interferometry shows that a thrust, subparallel to the Gowk fault and projecting to the surface about 30 km further east, also moved about 10 cm in a time interval and location which makes it likely that its slip was triggered by the 1998 March 14 earthquake. Third, the section of the Gowk fault system that moved in 1998, centred on Fandoqa, also produced coseismic surface ruptures during a larger (M_w 7.1) earthquake in 1981; however, whereas the smaller (M_w 6.6) 1998 earthquake produced horizontal offsets of up to 3 m, the larger (M_w 7.1) 1981 event produced much smaller surface offsets reaching only 0.4 m.

In the last 20 years five earthquakes on an 80 km section of the Gowk fault system have been associated with strike-slip surface ruptures. At least one of them (1998 March 14) is thought to have triggered slip (possibly aseismic) on adjacent thrusts. This sequence of events offers some insights into how a major oblique strike-slip and convergent fault system ruptures and also into how thrusts associated with such strike-slip systems can develop to create geological features often referred to as 'flower structures'.

The aims of this paper are therefore (1) to use field observations, seismology and SAR interferometry to investigate the faulting in the 1998 March 14 Fandoqa earthquake, (2) to re-assess the source parameters of earlier earthquakes on

the Gowk fault to see how they compare with the faulting in 1998, and (3) to understand how the complex faulting in these earthquakes is related to the regional active tectonics.

2 GEOLOGICAL AND TECTONIC SETTING

2.1 Topography

The Kerman province of SE Iran occupies a plateau typically 2000–2500 m in elevation, bordering the desert of the Dasht-e-Lut, where elevations are less than 500 m (Figs 1–3). The Kerman plateau itself is characterized by NW–SE to N–S trending ranges that are bounded by reverse and right-lateral strike-slip faults (see Figs 2 and 3 and Berberian 1981; Jackson & McKenzie 1984; Berberian & Yeats 1999). A set of ranges 50 km wide forms the edge of the plateau SE of Kerman (Figs 3 and 4), separating it from the Dasht-e-Lut. These ranges are cut by the Gowk fault, which is the subject of this paper. The Gowk fault system is marked by a narrow linear valley that joins several deep depressions: from north to south, at Chahar Farsakh, Jowshan-Hashtadan, Fandoqa, Golbaf and South Golbaf (Figs 5 and 6). The total length of the fault system is about 160 km, from the southern end of the Nayband fault in the north to the Jebel Barez mountains in the south (Fig. 3). At its northern end ($\sim 30.5^\circ\text{N}$) it turns NW and at its southern end ($\sim 29.3^\circ\text{N}$) it turns SE, in both places apparently acquiring a reverse component.

The Gowk valley and its associated faulting roughly follow the border between the Kerman plateau and the Dasht-e-Lut (Figs 3, 4 and 6), but are not a single structure at the base of the topographic slope. West of the valley, mountains rise to heights

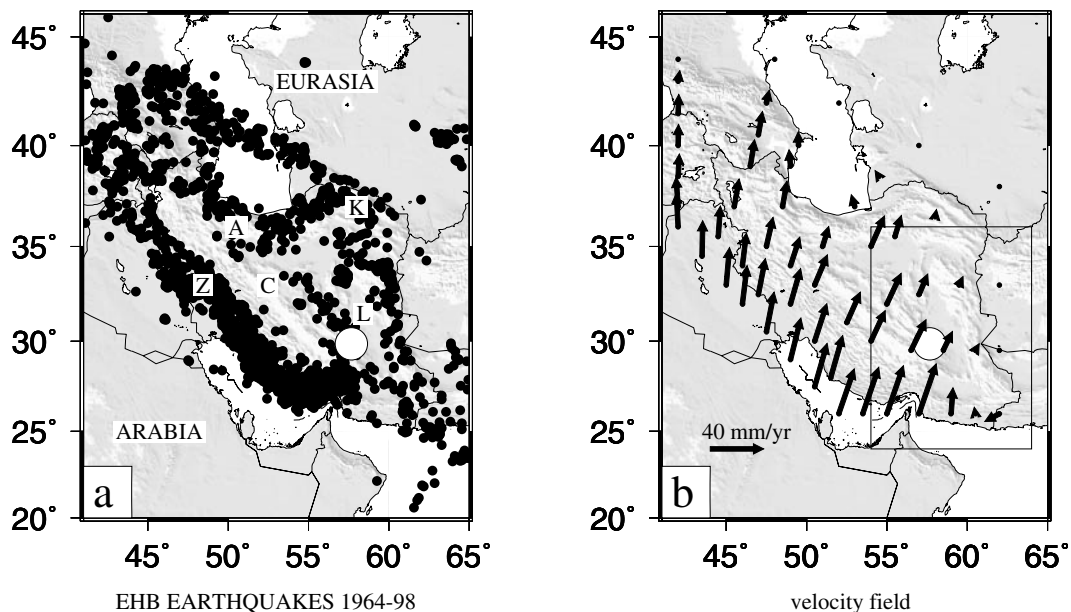


Figure 1. (a) Seismicity of Iran 1964–1998, with epicentres from the catalogue of Engdahl *et al.* (1998). Note how the cut-off in seismicity follows the NE and E borders of Iran. The Zagros is marked by Z, the Alborz by A, the Kopeh Dagh by K, the relatively aseismic central Iran block by C, and the Lut block by L. The 1998 Fandoqa epicentral region is marked with a white circle on both maps. (b) A velocity field for Iran showing how the NNE motion of Arabia relative to Asia is absorbed in Iran. The distribution of velocities within Iran is estimated from the spatial variation in the style of strain rates indicated by earthquakes (from Jackson *et al.* 1995). Note the expected right-lateral shear and shortening along the eastern border of Iran. The boxed region is the area shown in Fig. 2.

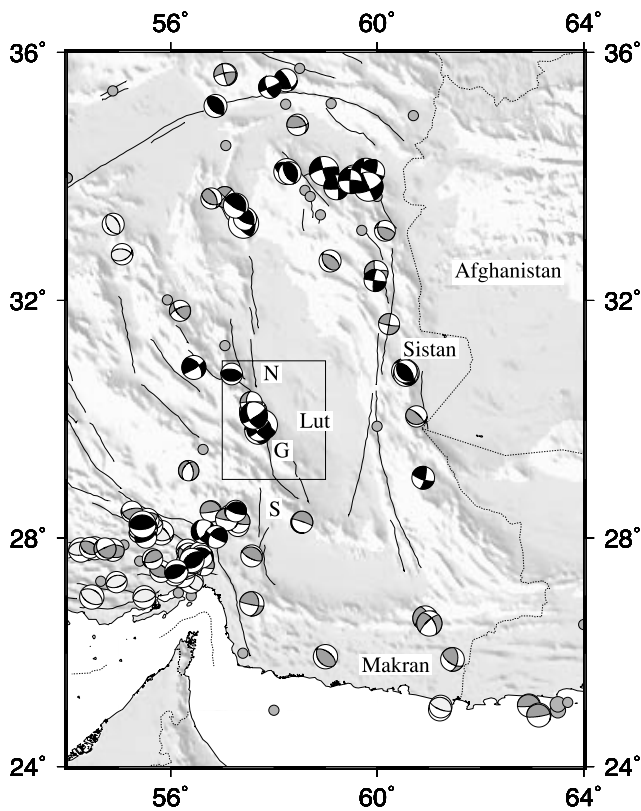


Figure 2. Regional summary map of faults and shallow earthquake focal mechanisms. Mechanisms constrained by body wave inversion (various sources) are in black, dark grey spheres are Harvard CMT solutions, and light grey spheres are first motion fault plane solutions from Jackson & McKenzie (1984). Gray circles are epicentres of 1900–1963 earthquakes with $M_s \geq 5.7$. Sub-crustal earthquakes associated with the Makran subduction zone have been removed. Faults are from Berberian & Yeats (1999). The boxed region is the area of Fig. 3. The Nayband, Gowk and Sabzevaran faults are marked N, G and S.

of 4200 m, at least 1500 m above the plateau level (Fig. 4). East of the valley there are also steep mountains, which reach heights of 2700 m. The valley floor itself is typically at elevations of 1700–2000 m and rises above the much lower desert floor to the east (200–500 m). In cross-section, the Gowk valley is asymmetric, with relatively long gentle slopes on the west side but abrupt steep slopes on its eastern margin. Young (probably Holocene) faulting is concentrated on the eastern side of the valley north of Golbaf (Fig. 6), and includes both east-facing and west-facing escarpments that are often discontinuous and obscured in areas where alluvial processes are active. South of the South Golbaf depression (Fig. 6) the youngest faulting is concentrated on the west side of the Gowk valley. The area is arid, but some of the depressions are reasonably well-supplied with water from mountain streams and springs, and population is concentrated in these locations. Gowk is the old name for the modern town of Golbaf, which takes its name ('Gol' = *lit.* flower) from the carpet-weaving and design motif for which the region is famous.

2.2 Geological setting

The East Kerman Ranges SE of Kerman are cut by the Gowk fault system (Fig. 3). The Sekonj mountains west of

the Gowk fault are formed of gently folded Mesozoic and Tertiary sediments, with a continuous sedimentary sequence from the Senonian passing into Palaeocene flysch deposition and with no evidence of volcanic activity. The oldest exposed rocks in the region are Jurassic siltstones and sandstones cropping out west of the fault. The Abbarik mountains east of the Gowk fault are mostly tightly folded and faulted Cretaceous sediments and Eocene volcanic rocks, with the Cretaceous rocks thrust eastwards over the Eocene pyroclastic deposits of a Palaeogene magmatic-arc assemblage. The Late Cretaceous–Palaeocene flysch deposits west of the Gowk fault are not found on its eastern side. The thick late Precambrian to early Cambrian salt deposits that occur in the Zagros mountains of SW Iran are not known in this region, although salt of an equivalent age is exposed in the mountains 75 km NW of Shahdad (Fig. 3) and roughly 20 km west of the Nayband fault.

The Dasht-e-Lut desert (Figs 2 and 3) is a low area of $\sim 400 \times 200 \text{ km}^2$ that has been an apparently stable block throughout much of the Tertiary, with a substratum of flat-lying Palaeocene andesitic lavas and tuffs. West of 59°E the prevailing winds and episodic floods have carved the Neogene silts into the famous Shahr-e-Lut (*lit.* 'the city of Lut') yardangs, which are ridges and mesas of salt-cemented silt up to 200 m high. East of 59°E the Lut is covered by huge sand dunes. The depression is fringed by terraces and gravel fans formed from Eocene volcanic domes. On its western side it is bounded by the Nayband fault, along which are numerous Quaternary basalt flows, and by the marginal Neogene fold-and-thrust belt between Shahdad and Keshit (Figs 3 and 6), which is developed in late orogenic continental molasse deposits that may be up to 3000 m thick and are composed of well-stratified marls containing gypsum, sandstones and conglomerates. These deposits overlap the Mesozoic and early Tertiary rocks of the Abbarik mountains east of the Gowk valley.

2.3 Active tectonics

Active faulting in Iran is related to the convergence between the Eurasia and Arabia plates, which occurs at about 40 mm yr^{-1} at longitude 60°E and is mostly accommodated by distributed shortening within the political borders of Iran. While much of this shortening is taken up in the main earthquake and mountain belts of the Zagros, Alborz and Kopeh Dagh (Fig. 1; Jackson *et al.* 1995), some is also accommodated in central Iran, of which the Kerman plateau is part. The low elevation and apparent lack of seismicity in the Dasht-e-Lut suggest that the Lut block is a relatively rigid block within this distributed deforming zone. Some of the roughly N–S right-lateral shear between central Iran and Afghanistan (which is essentially part of Eurasia) occurs on the long N–S strike-slip faults of Sistan near the Iran–Afghan border (Fig. 2 and Berberian *et al.* 2000) but some is also taken up on right-lateral faults striking N–S to NNW–SSE on the western side of the Lut block, of which the Gowk fault is one. There are no reliable estimates of slip rates on these strike-slip systems. If the Zagros accounts for roughly half the 40 mm yr^{-1} Arabia–Eurasia convergence (e.g. Jackson & McKenzie 1984; Jackson *et al.* 1995) then the remaining 20 mm yr^{-1} that is taken up within central and northern Iran will require $\sim 20 \text{ mm yr}^{-1}$ of strike-slip to be accommodated on the faults either side of the Lut block. In this case, a slip rate of several millimetres per year on the Gowk fault seems likely, but this estimate is very uncertain.

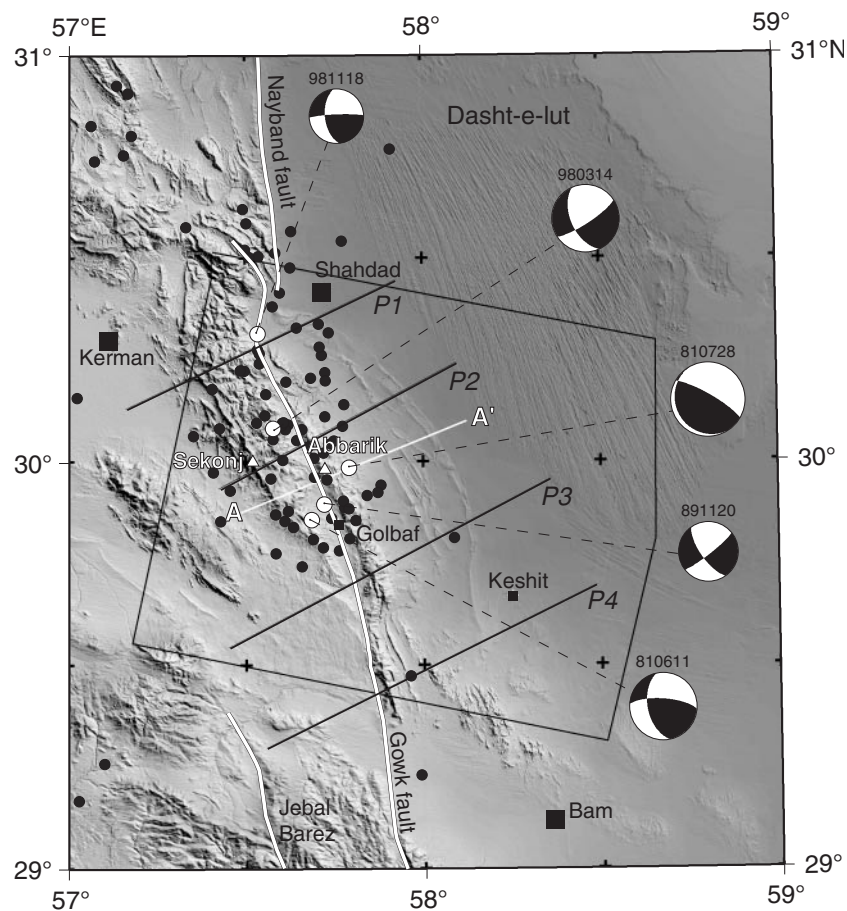


Figure 3. Summary map of the faulting, topography and focal mechanisms in the Gowk Fault zone. Thick white lines are the positions of the Nayband, Gowk and Sabzevaran faults (see Fig. 2). Large white circles are the approximate epicentres of the five main earthquakes whose source parameters are discussed in this paper (Table 1). Small black circles are other earthquakes from the catalogue of by Engdahl *et al.* (1998) for the period 1964–1998. Lines P1–P4 are the positions of the topographic profiles in Fig. 4, and the box outlines the area of the SAR images in Fig. 12. The line A–A' shows the location of the cross-section in Fig. 13.

2.4 Previous earthquakes on the Gowk fault system

Modern attention was first drawn to the Gowk fault system by two earthquakes in 1981 (Fig. 5 and Berberian *et al.* 1984). The 1981 June 11 Golbaf earthquake (M_w 6.6) produced surface ruptures for 15 km south of Zamanabad (Fig. 5) and was followed by the 1981 July 28 Sirch earthquake (M_w 7.1), which was associated with 65 km of discontinuous surface ruptures north of Zamanabad. The area south of Zamanabad then ruptured again in the 1989 November 20 South Golbaf earthquake (M_w 5.8), whose 11 km of surface ruptures followed the scarps formed in the 1981 June 11 earthquake exactly (Berberian & Qorashi 1994). The 1998 March 14 Fandoqa earthquake (M_w 6.6) again ruptured the 20 km north of Zamanabad with co-seismic surface faulting following that observed after 1981 July 28. Finally, a small (M_w 5.4) earthquake (1998 November 18) near Chahar Farsakh produced minor surface cracking over about 4 km, again along the scarp of the 1981 July 28 earthquake.

An interesting feature of this sequence is the gap in damage distribution and fault movement near the village of Zamanabad. In both large earthquakes of 1981 and in the 1998 Fandoqa earthquake, co-seismic surface displacement died out near Zamanabad, which is also a region where the earlier scarps on the Gowk fault system seem less obvious and well-developed.

Other earthquakes in the region are known from historical records, but it is usually difficult to associate them with particular faults. Those since 1850 are shown in Fig. 5. All of them are smaller than the larger events of 1981 and 1998 and damaged relatively restricted areas. Those that can plausibly be related to the Gowk fault have their approximate damage regions marked on that assumption. From Fig. 5 it can be seen that there is more evidence for pre-1981 seismicity north of Zamanabad than to the south. By contrast, the long strike-slip faults to the north (Nayband) and south of the Gowk fault are not associated with any known large earthquakes in historical times (Ambraseys & Melville 1982; Berberian & Yeats 1999).

3 THE 1998 MARCH 14 FANDOQA EARTHQUAKE (M_w 6.6)

3.1 Overview and macroseismic effects

The 1998 March 14 Fandoqa earthquake occurred at 19:40 GMT (23:10 local time on 23 Esfand 1376 of the Iranian calendar), with no warning foreshock activity. The earthquake killed five people in Golbaf (official figure), injured 15, and damaged seven villages [Golbaf (MMI intensity VII), Zamanabad (VII), Fandoqa (VII), Hashtadan (VII), Jowshan (VI), Dehu (VI) and

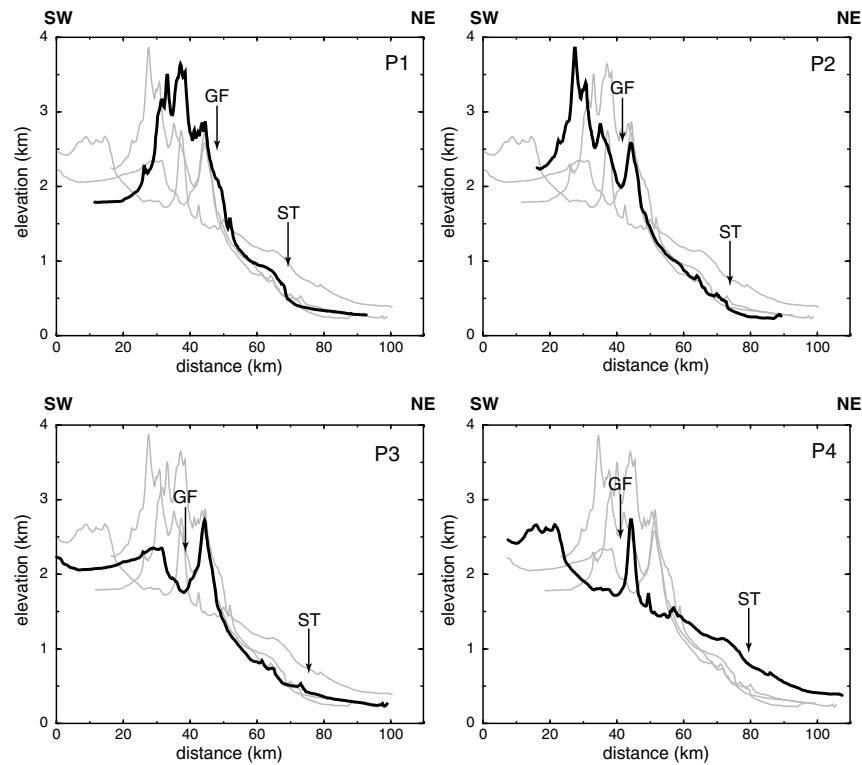


Figure 4. Topographic swath profiles (500 m wide) crossing the Gowk fault zone along the lines in Fig. 3, showing the elevation contrast between the Kerman plateau in the SW, the Dasht-e-Lut desert in the NE, and the mountains either side of the Gowk fault zone. The position of the Gowk Fault is marked GF. The frontal ridge of the Shahdad thrust system is marked ST. Each profile P1–P4 is shown in black, while the other profiles are in grey in each box to show the similarities and variations between their shapes. The profiles are aligned roughly on the position of the Shahdad thrust or the eastern flank of the Abbarik mountains.

Deh Qanbar (VI): see Fig. 7]. Damage was most severe to the traditional, heavily built, single-storey houses of weak masonry and non-reinforced adobe, with domed or flat wooden-beamed roofs, many of which collapsed in the earthquake. In addition, many non-reinforced free-standing concrete-block, brick, adobe or stone walls in courtyards in Golbaf also fell down. By contrast, reinforced structures built after the destruction of the 1981 earthquakes did not collapse. The 2.7 km-long tunnel linking the Kerman plateau to the Gowk valley near Sirch, which was under construction during the 1981 earthquakes, suffered no serious damage. However, water and power supplies in the epicentral area were severely disrupted and not restored until 36 hr after the earthquake. The shock was felt strongly in Mahan (V on MMI, 40 km west of Fandoqa), Rayen (V, 50 km SW), Shahdad (V, 50 km N), Kerman (IV, 70 km NW), Chatrud (III, 100 km NW) and Baft (III, 140 km SW). The closest strong-motion instrument that recorded the main shock was at Sirch (28 km N of Fandoqa), and registered 0.66g acceleration on the vertical component (Mirza'i-Alavicheh & Farzanegan 1998).

The main-shock was followed by numerous aftershocks, the strongest of which (m_b 4.9) was on 27 March 1998 at 16:20 GMT. On 19 October 1999 an earthquake of m_b 4.6 broke window panes, knocked over television sets and damaged the water supply at Golbaf. Finally, on 18 November 1998 an earthquake of M_w 5.4 damaged houses at Chahar Farsakh, 45 km N of the March 14 epicentral region and was associated with surface cracking near the north end of the Gowk fault system (discussed later).

3.2 Coseismic surface ruptures

The 1998 March 14 Fandoqa earthquake produced surface faulting along the Gowk valley between Hashtadan in the north and Zamanabad in the south (Figs 6b and 7), following the southern part of the surface ruptures observed in the larger Sirch earthquake of 1981 July 28 (Berberian *et al.* 1984). A smaller earthquake of M_s 6.1 affected a similar area centred on Fandoqa on 1948 July 5 (see Fig. 5 and Ambraseys & Melville 1982).

Three days after the 1998 Fandoqa earthquake the area was visited by M. Qorashi and M. Talebian and the general pattern of the ruptures was mapped at a scale of 1:50 000, using the 1955 (1:55 000) aerial photographs and topographic maps. The area was re-visited in April 1999 by M. Berberian and J. Jackson and with more recent (1:40 000) air photos. With no helicopter flights and no detailed post-earthquake air photos, we were unable to map details of all the fracture systems adjacent to the main surface fault. It is known that prior to the first site visit, heavy rain caused some small fractures to be covered with debris material.

The 1998 surface ruptures were predominantly right-lateral strike-slip in character, often accompanied by a vertical slip component (Fig. 8). The ruptures extended for a total length of 23.5 km along the eastern side of the Gowk valley with an overall strike of 156° . Of the 1998 ruptures about 14.25 km were east-facing and 9.25 km were west-facing. The west-facing sections were at both ends of the rupture zone and in the middle, in Fandoqa playa (Fig. 7). The surface ruptures were expressed

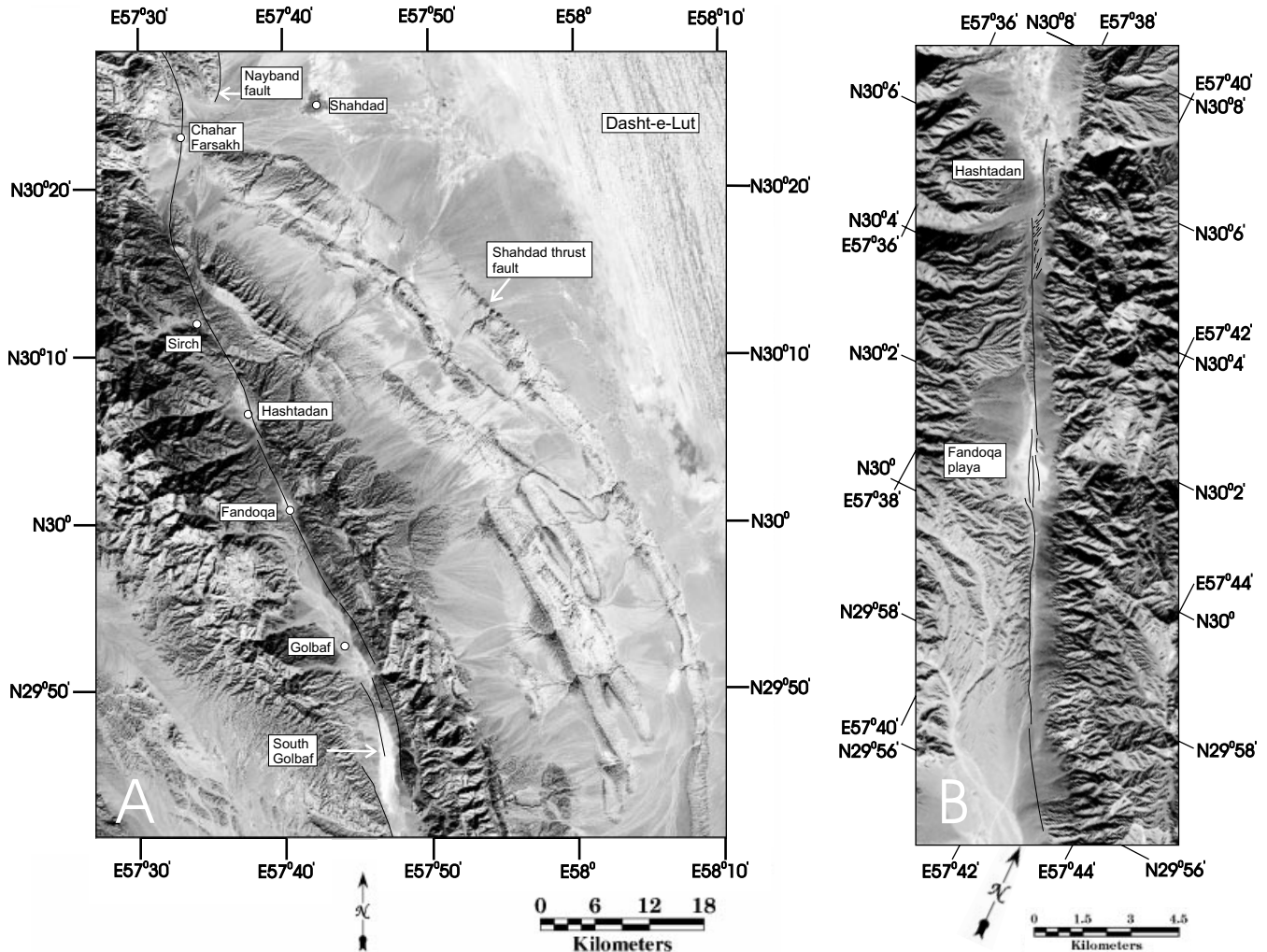


Figure 6. LANDSAT TM images of the Gowk fault zone. (a) The whole central part of the fault zone, from its junction with the southern tip of the Nayband Fault in the north to the south Golbaf depression in the south. This covers the entire rupture zones of the five 1981–1998 earthquakes whose focal mechanisms are shown in Fig. 3. Note the subparallel ridges formed by anticlines above the blind faults of the Shahdad thrust system in the east. (b) Detailed image of the rupture zone of the 1998 March 14 Fandoqa earthquake. Thin black lines in the Gowk valley indicate the principal coseismic surface faults (see also Fig. 7).

3.2.2 Linear scarps south of Hashtadan and south of Fandoqa

The clearest and most localized surface ruptures from the 1998 earthquake began about 5 km south of Hashtadan at an elevation of ~ 1900 m and continued to the northern edge of the Fandoqa playa, reaching an elevation of ~ 2000 m (Figs 6b, 7a, 9b and 9d). Another set of equally clear but smaller offset-ruptures ran from south of Fandoqa (elevation ~ 2100 m) to NE of Zamanabad (elevation ~ 2100 m). In both places the ruptures formed continuous, linear and narrow shear zones (usually less than 10 m wide) with a constant trend of 156° . Tension cracks within these zones were much shorter and more closely spaced than those observed in the playas. In both places the well-defined linear trace of the surface ruptures was developed at the foot of east-facing escarpments in dissected late Neogene conglomerates and sandstones or late Pleistocene alluvial fans (Figs 6b and 9b). These pre-existing escarpments all show well-developed incision of drainage on their western sides, indicating a longer-term uplift of the western relative to eastern blocks. Local fault dips, where visible, were typically

subvertical or steeply east-dipping on east-facing scarps, but in two places between Hashtadan and Fandoqa dips of 65° and 78° to the west were measured near the surface.

3.2.3 Small fractures near Zamanabad

For the southern 3.25 km of the 1998 surface faulting, starting 2.5 km N of Zamanabad, the sense of vertical movement along the ruptures changed from east- to west-facing. Along this section the ruptures were discontinuous and distributed fractures with typically only a few centimetres offset. The maximum horizontal and vertical displacement we recorded on any one fracture in this region were ~ 13 cm (Figs 6b, 7a and 8).

3.2.4 Coseismic slip measurements in 1998 and 1981

Fig. 8 shows a summary of 1998 and 1981 coseismic slip measurements. The values given are those measured along the main fault trace and do not include any additional offset distributed among the smaller ruptures in the fault zone. In some places they are, therefore, underestimates of the true coseismic

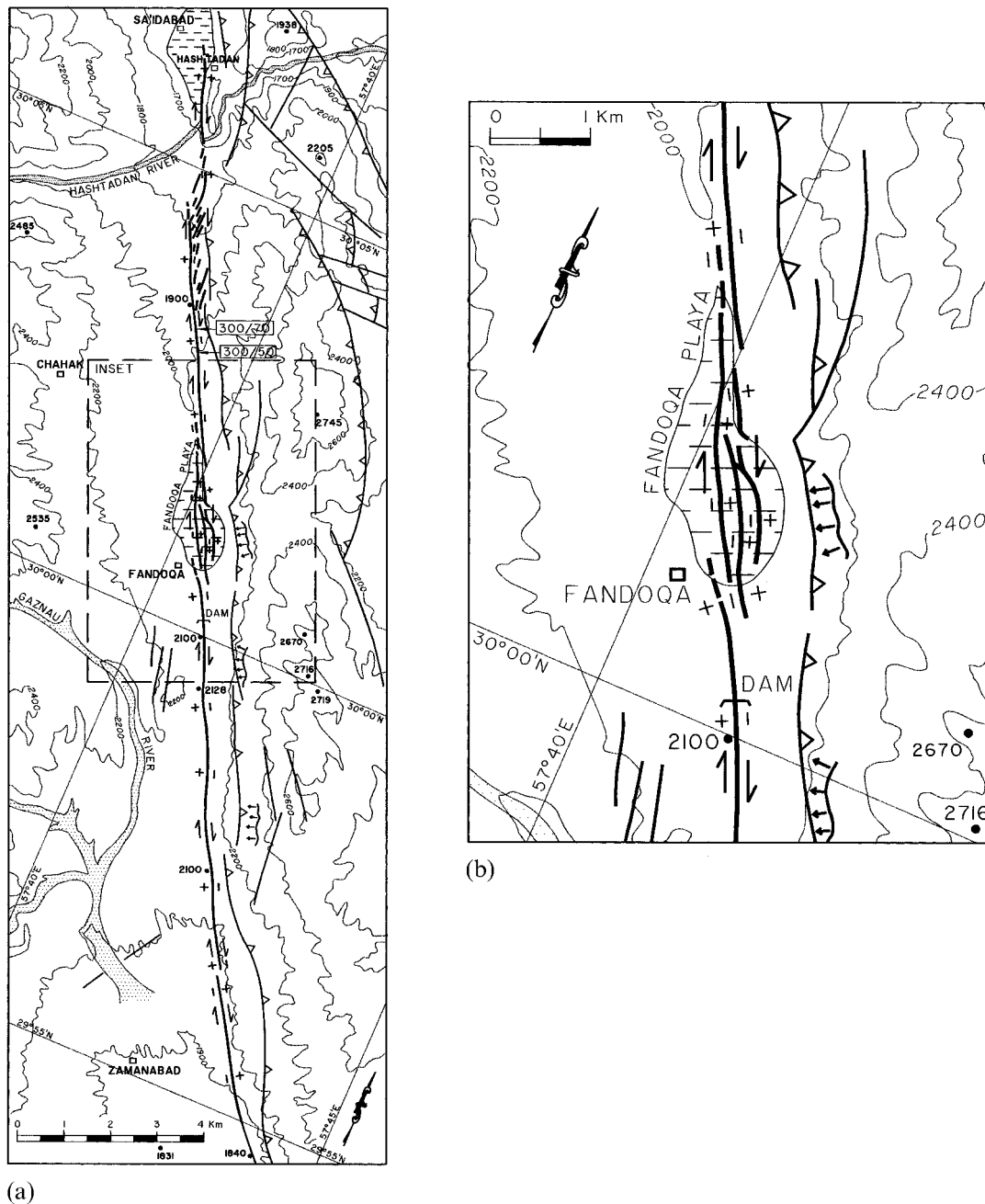


Figure 7. (a) Detailed map of the coseismic ruptures (thick lines) in the 1998 March 14 Fandoqa earthquake (see also Fig. 6b). Thin lines are other faults that showed no surface reactivation in 1998. Relative uplift and subsidence across the 1998 ruptures are marked by + or -. Groups of arrows on the east side of the valley are earthquake-triggered landslides. Numbers in the two boxes between Fandoqa and Hashtadan show the locations of maximum horizontal/vertical slip (in cm) in 1998. The Hashtadan and Fandoqa playas are marked by horizontal dashed lines. Elevations are in metres. Note the right-lateral offset and diversion of the Hashtadan river where it crosses the Gowk fault. (b) Detail of the ruptures near Fandoqa playa, covering the area of the box marked 'inset' in Fig. 7(a).

slip at the surface. The offsets in Fig. 8 were measured where the surface ruptures crossed ravines, distributaries, berms and furrows in agricultural fields (e.g. Figs 9e and g), tyre tracks, and other natural and man-made landmarks.

The magnitude of the horizontal strike-slip offset varied along the 1998 fault zone but was typically 1–2 m, with a maximum of 3 m in the area 5 km N of Fandoqa (Fig. 9c). The general pattern is that both strike-slip and vertical displacements were greatest in the northern half of the fault zone, diminishing rapidly to the north but more gradually to the

south (Fig. 8). In general, high values of strike-slip displacement occurred in places where the vertical component was also large.

For nearly all the distance from Hashtadan to Zamanabad the 1998 ruptures closely followed the trace of the surface faulting in the 1981 July 27 Sirch earthquake (Berberian *et al.* 1984), which was mapped in 1981 by two of the authors of this report (Qorashi and Berberian), who also observed the 1998 faulting. The exception is the southernmost 5 km of the 1998 ruptures, which apparently broke most of a 6.6 km gap that

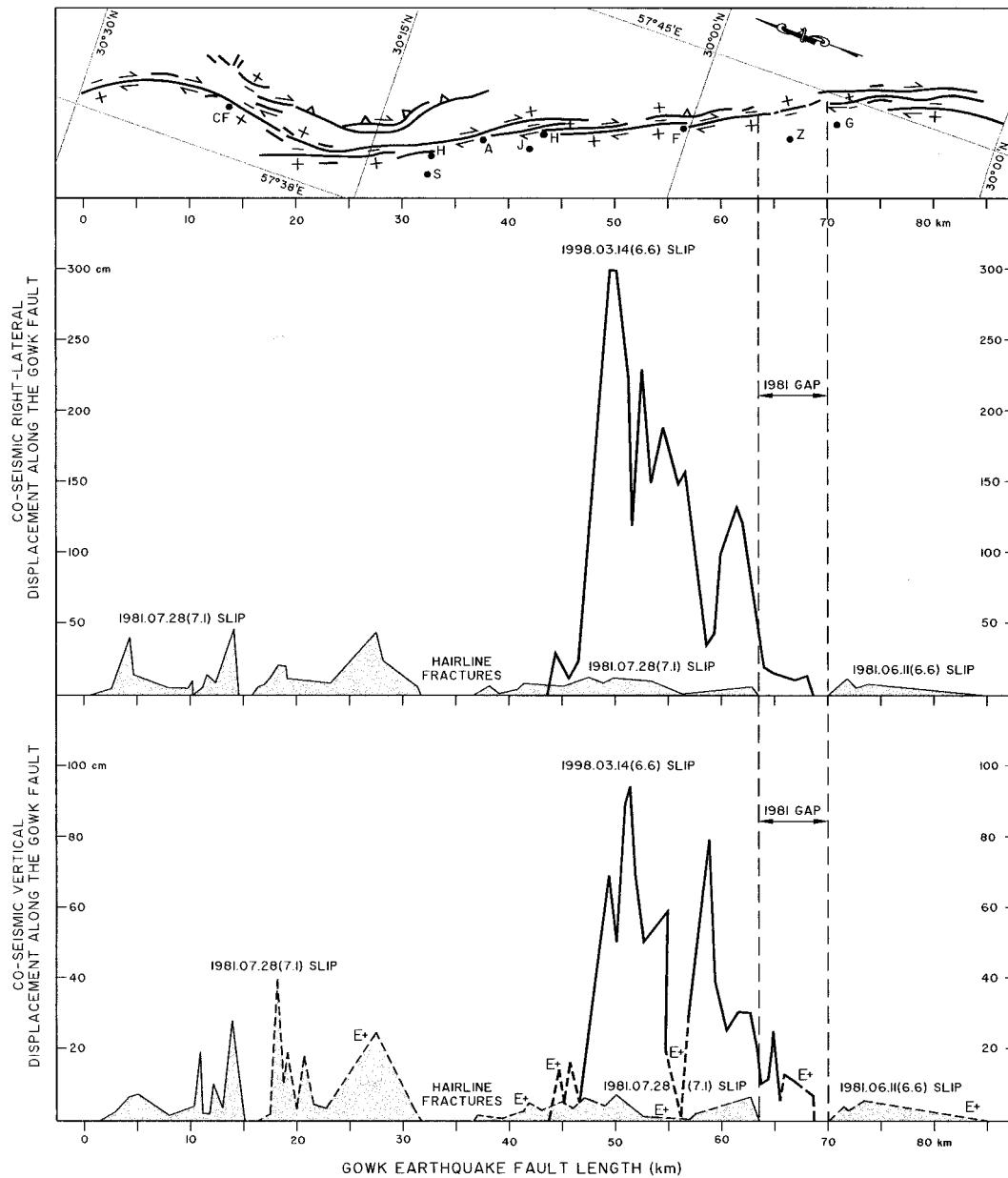


Figure 8. Observed amplitudes of coseismic right-lateral (middle) and vertical (bottom) offsets on the Gowk fault system following the 1981 June 11 Golbaf and 1981 July 28 Sirch earthquakes (thin lines, shaded) and the 1998 March 14 Fandoqa earthquake (thick lines). Offsets are in centimetres, plotted against distance along the fault measured on the map in the top panel. Where coseismic fault segments from the same earthquake overlapped, their cumulative value has been plotted. In the bottom panel, dashed lines, marked E+, indicate that the vertical sense of slip was east-side-up. Observed points at which offsets were measured have been joined by lines to distinguish the 1981 and 1998 displacements, and not to imply that the offsets varied between those points in the jagged manner indicated by the profiles. Note the large offsets from the M_w 6.6 Fandoqa (1998) earthquake compared with the much bigger ($\sim M_w$ 7.1) 1981 Sirch earthquake. Z is Zamanabad, A is Ab-e-Garm, CF is Chahar Farsakh, H in the north is Hasanabad, H in the south is Hashtadan, S is Sirch, F is Fandoqa, G is Golbaf and J is Jowshan.

separated the coseismic surface faulting in the 1981 June 11 (Golbaf) and 1981 July 27 (Sirch) earthquakes (see Fig. 8 and Berberian *et al.* 1984).

However, the magnitude of the strike-slip and vertical offsets seen at the surface in the 1998 March 14 Fandoqa earthquake (M_w 6.6) were consistently greater than those measured after the much larger 1981 July 27 Sirch earthquake (M_w 7.1). The maximum strike slip and vertical slip observed in 1998 were 300 and 95 cm respectively, compared with 43 and 40 cm respectively in 1981 (Figs 8 and 19). Moreover, whereas a maxi-

imum of 300 cm strike-slip offset was observed in 1998, only 13 cm was observed in 1981. We return to this discrepancy later.

3.3 Earthquake source parameters: seismology

To provide better constraints on the source parameters of the 1998 March 14 Fandoqa earthquake we analysed the *P* and *SH* body waveforms. We took digital broad-band records from stations of the GDSN in the epicentral range 30° – 90° and

convolved them with a filter that reproduces the bandwidth of the old WWSSN 15–100 long period instruments. We then used the MT5 version (Zwick *et al.* 1994) of McCaffrey & Abers's (1988) and McCaffrey *et al.*'s (1991) algorithm, which inverts the *P* and *SH* waveform data to obtain the strike, dip, rake, centroid depth, seismic moment and source time function, which is parametrized by a series of isosceles triangle elements of half-duration τ s. We always constrained the source to be a double-couple. The method and approach we used are described in detail elsewhere (e.g. Nabelek 1984; McCaffrey & Nabelek 1987; Molnar & Lyon-Caen 1989; Taymaz *et al.* 1991) and are too routine to justify repetition here.

The results of this inversion are shown in Fig. 10 and Table 1. The solution indicates right-lateral strike slip on a fault dipping 54° WSW, with a strike of 156° that is almost identical to the overall trend of the coseismic ruptures observed at the surface. With abundant clear seismograms and a good azimuthal coverage of stations recording both *P* and *SH* the solution is, in general, well-constrained. To estimate uncertainties in source parameters we carried out tests in which one parameter was held fixed at values different from that in the final solution of Fig. 10, while the other parameters remained free in the inversion. We then examined how far the value of the fixed parameter could be shifted before there was a substantial visual degradation in the fit between synthetic and observed seismograms. This methodology is illustrated in greater detail in Molnar & Lyon-Caen (1989) and Taymaz *et al.* (1991). In this way we estimated the uncertainties to be approximately $+10^\circ/-15^\circ$ in strike, $\pm 10^\circ$ in dip, $\pm 15^\circ$ in rake and ± 2 km in centroid depth. As usual for shallow earthquakes there is some trade-off between depth and seismic moment, with shallower

depths requiring higher moments to fit the observed seismograms. We carried out the inversion in a half space with $V_p = 6.5$ km s $^{-1}$ and $V_s = 3.7$ km s $^{-1}$. Realistic changes in the velocity model make little change to the source orientation or depth, but can affect the seismic moment. We estimate the uncertainty in moment to be less than 2.0×10^{18} N m or ~ 20 per cent.

Our inversion solution is similar in orientation and magnitude to that of the 'best-double-couple solution' in the Harvard CMT catalogue (Table 1). However, the Harvard CMT solution is not constrained to be a double-couple source and in fact has a substantial non-double-couple component, with eigenvalues of 10.7, -2.6 and -8.1×10^{18} N m (see also Table 1). One explanation for this could be that the earthquake involved rupture in two or more discrete subevents with different orientations (see e.g. Berberian *et al.* 1984, who suggest this as an explanation for the large non-double-couple components in the 1981 Golbaf and Sirch earthquakes, which we discuss later). Our inversion in Fig. 10 indeed shows a rather jagged source time function, including two short pulses after the main moment release in the first 6 s. In Fig. 11 we show why the time function has this character. This figure shows a selection of *P* and *SH* waveforms at different stations for the 1998 Fandoqa earthquake. The first line is our final inversion solution for this event. The second line is a solution in which the length of the time function has been restricted to 6 s, but all the source parameters are otherwise free to change. The inversion finds it difficult to match the width of the first full cycle of the *P* waveforms, particularly at stations to the NE (e.g. YAK), and attempts to achieve this by increasing the depth, but cannot increase the depth beyond 7 km without also affecting the *SH*

Table 1. Source parameters of the main Gowk valley earthquakes. Epicentres are from Engdahl *et al.* (1998). Magnitudes (m_b and M_s) are from the USGS. An **m** after the M_w value indicates that two subevents were required to model the body waves. Seismic moment (M_0) is in units of 10^{18} N m. TF is the duration of the time function in seconds (the time for 95 per cent of the seismic moment to be released), and sv is the slip vector azimuth, assuming that the west-dipping nodal plane is the fault plane. The last column gives the origin of the earthquake source parameters on each line: from body wave modelling in this paper (B, shown in bold type, with B1 and B2 signifying the first and second subevents in the 1981 June 11 earthquake), or from the CMT solutions by Harvard (H) or the USGS (U). The * after the Harvard CMT depth indicates that it was fixed at 15 km in the inversion. The number in brackets after the H or U in the last column indicates the extent to which the CMT solution can be represented by a double-couple source, expressed as a percentage (γ) according to the formula $\gamma = 100\{1 - [(2|\lambda_2| \times 1.5)/(|\lambda_1| + |\lambda_3|)]\}$, where λ_1 , λ_2 and λ_3 are the maximum, intermediate and minimum eigenvalues of moment tensor. In this (arbitrary) definition, $\gamma = 100\%$ for a pure double-couple source (e.g. with eigenvalues $-1, 0, +1$) and 0 per cent for a linear vector dipole (e.g. with eigenvalues $-0.5, -0.5, +1.0$).

Date	Time	Lat.	Long.	Depth	m_b	M_s	M_w	M_0	Strike	Dip	Rake	TF	sv	R
1981.06.11 (Golbaf)	07:24:24	29.86	57.68	20	6.1	6.7	6.58m	4.18	169	52	156	3.9	184	B1
				12				5.30	182	88	198	8.6	182	B2†
				20				6.59	9.82	172	37	171	179	H(57)
				8				6.59	9.73	169	22	142	206	U(98)
1981.07.28 (Sirch)	17:22:24	29.99	57.79	18	5.7	7.1	6.98	36.69	177	69	184	47.1	176	B
				15				7.24	90.10	150	13	119	210	H(76)
				22				7.02	43.20	293	67	115	153	U(98)
1989.11.20 (S. Golbaf)	04:19:07	29.90	57.72	10	5.6	5.5	5.83	0.70	145	69	188	4.0	142	B
				15*				5.88	0.82	148	81	165	150	H(79)
1998.03.14 (Fandoqa)	19:40:28	30.08	57.58	5	5.9	6.9	6.57	9.09	156	54	195	9.4	147	B
				15*				6.58	9.43	154	57	186	151	H(59)
				8				6.52	7.70	146	58	181	146	U(99)
1998.11.18 (C. Farsakh)	07:39:27	30.32	57.53	15*	4.9	5.1	5.34	0.13	174	55	173	178	H(97)	

† second subevent 2.2 s after the first, offset 8.1 km in direction 256° .

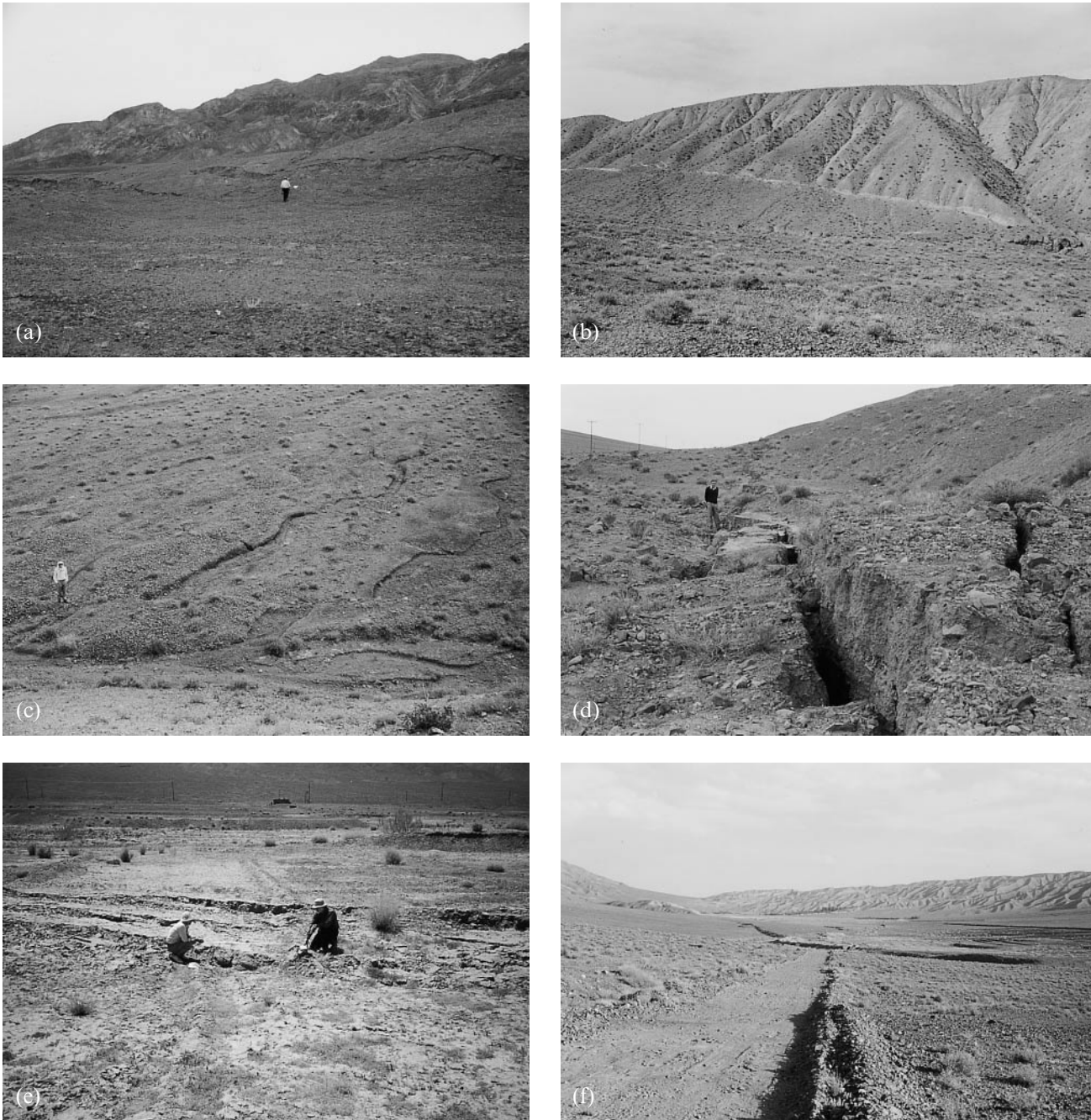


Figure 9. Field photographs of coseismic surface ruptures and geomorphology following the 1998 March 14 Fandoqa earthquake. (e) was taken in April 1999. All the others were taken in March 1998, a few days after the 1998 Fandoqa earthquake. (a) View E of west-facing, left-stepping en echelon scarps about 500 m south of the Hashtadan river. (b) View west of the east-facing scarp south of Hashtadan at $30^{\circ}03.28'N$ $57^{\circ}39.09'E$, near the location of maximum offset shown by the boxes in Fig. 7(a). (c) View east in the same area as 9(b). The person is standing on the fault trace, which has offset gullies ~ 2.5 m in a right-lateral sense. (d) View south of the east-facing scarp in the same region as 9(b) and 9(c). (e) View W of a 2 m right-lateral offset in a field boundary (between the two people) in the northern part of the Fandoqa depression at $30^{\circ}02.15'N$ $57^{\circ}39.78'E$. (f) Overview of the Fandoqa depression, looking SW from its northern end. The scarp crossing the road is up on its western side but loses this vertical component before following the western (right) side of the bluff in the distance. The location of 9e is between the bluff and the road. (g) A field boundary offset 1.5 m (between the white markers) in the Fandoqa playa. View W to Fandoqa village in the background. (h) A shattered zone of en echelon cracks and fissures in the Fandoqa playa, on the west side of the bluff in 9(f). View south to the pass containing an earth dam (see Fig. 7a). (i) View north of a gorge cutting through the frontal anticline of the Shahdad thrust system, south of Shahdad at $30^{\circ}19.16'N$ $57^{\circ}46.01'E$. Note the folding of the surface gravels and the incision of the river. (j) Detail of the west side of the gorge at 9(i), near its exit onto the Shahdad plain. Small, west-dipping thrusts (which were checked, and had not moved, after the 1981 and 1998 earthquakes) are seen cutting the uplifted and folded gravels.



Figure 9. (Continued.)

waveforms. We conclude that some additional moment release is required beyond the first 6 s of the time function, particularly to match the double-upward pulse at all stations to the NE such as YAK (see Fig. 10). We return to the rest of Fig. 11 later.

3.4 Earthquake source parameters: radar interferometry

SAR interferometry is now established as a valuable technique for studying ground movements caused by earthquakes (e.g. Massonnet *et al.* 1993; Massonnet & Fiegl 1998). The principle uses phase information from SAR images of the ground surface, acquired before and after an event in which ground displacements have occurred, to generate an interferogram representing the change in line-of-sight displacement between the satellite and the ground. The technique provides high spatial sampling and subcentimetre precision, with each fringe in the interferogram corresponding to 28 mm of displacement in the line-of-sight direction.

To investigate the 1998 March 14 Fandoqa earthquake, we used two ERS-2 SAR images spanning a time interval of 28 months (Table 2). We used the ROI-pac software to create an interferogram with ~ 80 m pixels, using precise orbits determined by the German DPAF. Topographic contributions to the interferogram were removed using a 3 arc-second resolution digital elevation model and the result was then smoothed using a power spectrum filter. The corrected interferogram is shown in Fig. 12(a). Coherence in the interferogram is best over the moderate relief on the sides of the Gowk valley and on the edge of the desert and is relatively poor in the high topography and close to the Gowk fault itself. The basic pattern shows 19 fringes west of the Gowk fault and nine fringes to the east of the fault, with two of the eastern fringes extending 20–30 km further east over the Shahdad thrusts bordering the Dasht-e-Lut, which we discuss later.

We used the fringes in Fig. 12(a) to estimate source parameters in the 1998 March 14 Fandoqa earthquake, assuming

Table 2. Details of ERS-2 data used in this study. All SAR data copyright ESA.

Interferogram location*	Date 1	Orbit 1	Date 2	Orbit 2	h_a^\dagger
Track 392, frame 3004	27 May 1996	5757	14 Sept 1998	17781	149 m

(*) At the middle of the Fandoqa fault break within this frame, the inclination angle is $\sim 25^\circ$, and the unit vector \hat{n} pointing towards the spacecraft is $\hat{n} = (0.419, -0.087, 0.904)$ in the coordinate system (east, north, up), i.e. the spacecraft moves almost from north to south with the SAR looking to the right or west.

(†) The altitude of ambiguity, the magnitude of topographic error required to cause a single interference fringe, again estimated at the centre of the fault.

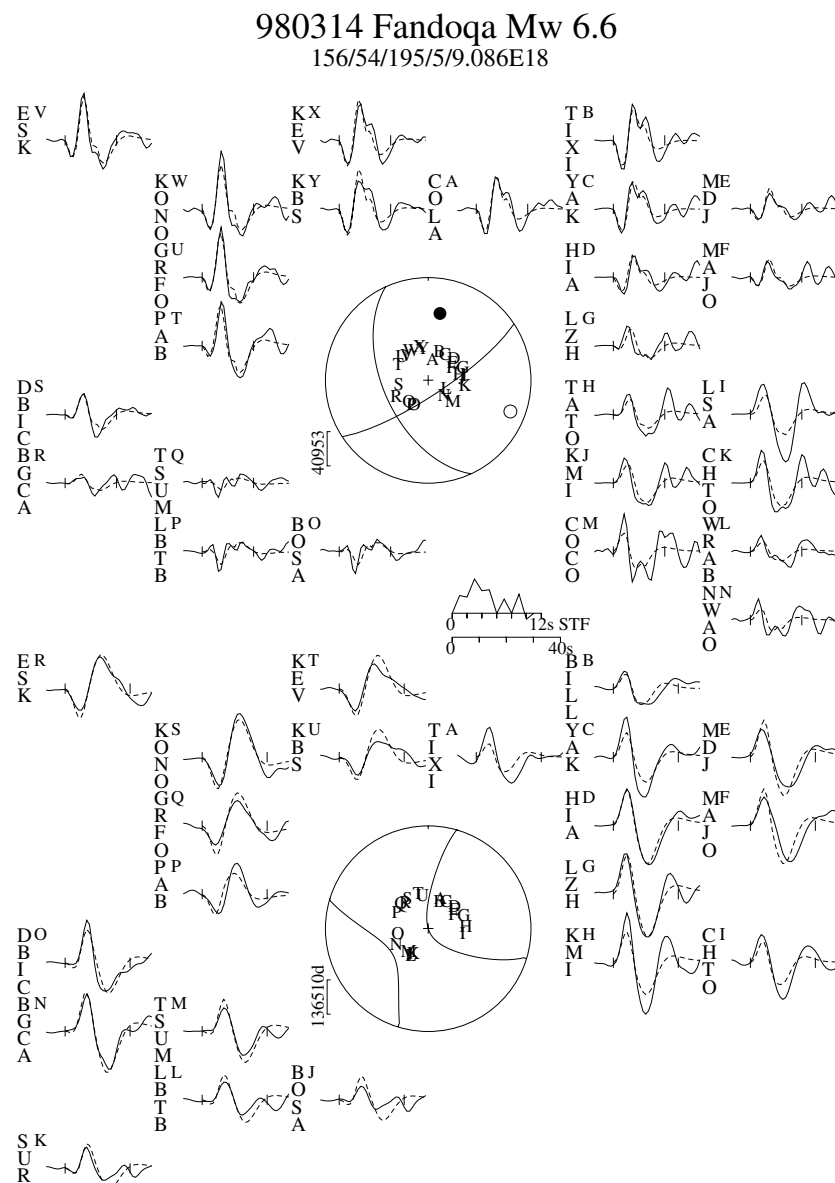


Figure 10. *P* (top) and *SH* (bottom) observed (solid) and synthetic (dashed) waveforms for the 1998 March 14 Fandoqa earthquake (Table 1). Station positions on focal spheres are identified by capital letters and arranged clockwise starting from north. STF is the source time function. Vertical ticks on the seismograms indicate the inversion window. Numbers beneath the header line are strike, dip, rake, centroid depth (km) and moment (N m). Stations were weighted according to azimuthal density and then the *S* seismogram weights were halved, to compensate for their larger amplitudes.

that all ground displacement occurred during the earthquake and was caused by uniform slip on a planar, rectangular fault surface in an elastic half-space. The approach we used follows that described in Wright *et al.* (1999). The surface displacement vector (\mathbf{u}) at each point caused by the elastic dislocation was calculated using the expressions in Okada (1985) and then projected into a line-of-sight displacement ($\Delta l = \hat{\mathbf{n}} \cdot \mathbf{u}$), where $\hat{\mathbf{n}}$ is the unit vector in the line of sight (Table 2). We then use a hybrid Monte-Carlo, downhill simplex inversion technique, described in Clarke *et al.* (1997) and Wright *et al.* (1999), to calculate a model that provides a best fit to line-of-sight displacements digitized at 507 discrete locations along identifiable fringe boundaries. The inversion determines 10 parameters in all for the single dislocation solution: strike, dip, rake, amount

of slip, latitude and longitude at the centre of the surface intersection of the fault plane, length of scarp, minimum and maximum fault depth, and a line-of-sight offset to allow for an incorrect assignment of the zero-displacement fringe.

The source parameters from our inversion of the observed SAR fringes (Table 3) are used to create a synthetic interferogram (Fig. 12b). In fact, Fig. 12(b) also includes synthetic fringes designed to match those observed over the Shahdad thrusts in the east, which we discuss later. Some source parameters are better resolved than others, and an appreciation of our inversion's limitations requires some discussion of the general features of the interferogram. The orientation of the fault is tightly constrained by the points close to the ends of the fault where the opposite lobes of the fringe pattern come together.

Table 3. Source parameters of the 1998 Fandoqa earthquake from SAR and seismology. Source parameters estimated from SAR interferometry were calculated using Lamé elastic constants $\lambda=3.22 \times 10^{10}$ Pa and $\mu=3.43 \times 10^{10}$ Pa. Column 1 shows the results from an inversion in which all parameters were free to change. In the inversion shown in column 2 the rake was fixed at 180° (pure right-lateral strike-slip). The source parameters from the seismological inversion (Fig. 10, Table 1) are shown for comparison in column 3: the slip was calculated from the moment and fault area, assuming a length from the surface ruptures and a depth equal to twice the centroid depth. The n or t after the dip-slip component indicates normal or thrust slip. The last column shows the result of a free inversion for the fringes on the Shahdad thrust. The dip of the Shahdad fault determined by SAR is given as 8°W^* and is actually the angle between the fault and the ground surface, which slopes 2° to the east, so that the fault dip is 6°W relative to the horizontal.

	Gowk fault			Shahdad thrust
	SAR free (1)	SAR rake fixed (2)	Seismic free (3)	SAR free (4)
Strike	150	150	156	159
Dip	52	56	54	8^*
Rake	214	180	195	95
Total slip (m)	1.34	3.27	1.29	0.076
Strike-slip component (m)	1.11	3.27	1.24	0.007
Dip-slip component (m)	0.75n	0.00	0.33n	0.076t
Depth to top (km)	0.22	0.02	(0)	1.63
Depth to bottom (km)	7.11	5.98	(10)	4.83
Fault length (km)	20.7	20.3	(23.5)	35.0
Fault area (km ²)	180.2	146.7	235	768
Moment ($\times 10^{18}$ N m)	8.28	16.45	9.09	2.00

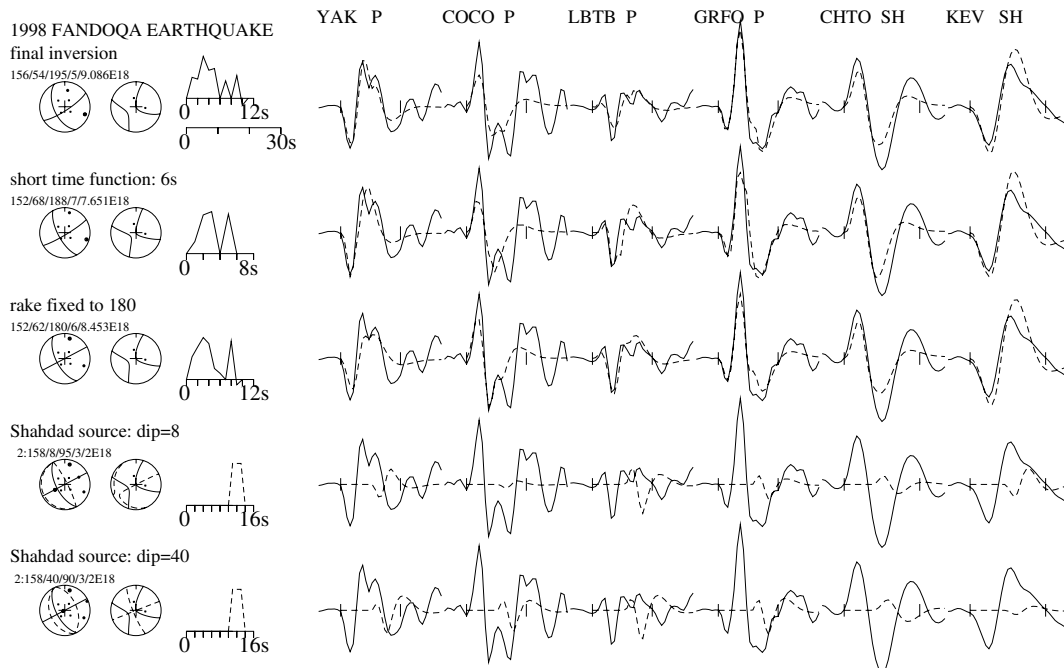


Figure 11. Tests to check the inversion for the 1998 March 14 earthquake (Fig. 10) for sensitivity to source time function duration, rake and possible later ruptures on the Shahdad thrust system (see text). Synthetic seismograms are dashed, observed are solid lines. The first line contains seismograms at selected stations from Fig. 10, the final inversion result. *P* and *SH* focal spheres are shown, with the time function and numbers showing the strike, dip, rake, depth and moment. In the second line the time function duration was restricted to 6 s, with all other parameters left free in the inversion. In the third line the rake was fixed to 180° (pure strike-slip) with other parameters free. The resulting solution violates the clear downward first motion at LZH. If the rake is fixed to 160° (to require a thrust component of slip) many first motions are violated in the NE (see Fig. 10). The fourth line is a forward model, showing the effect of a rupture 10 s after the first motion, with the orientation of the thrust found from the SAR data beneath the Shahdad anticlines (Table 3) and a short time function of duration 4 s. The fifth line shows a forward model with the same parameters as in line 4, but with the dip steepened to 40°W .

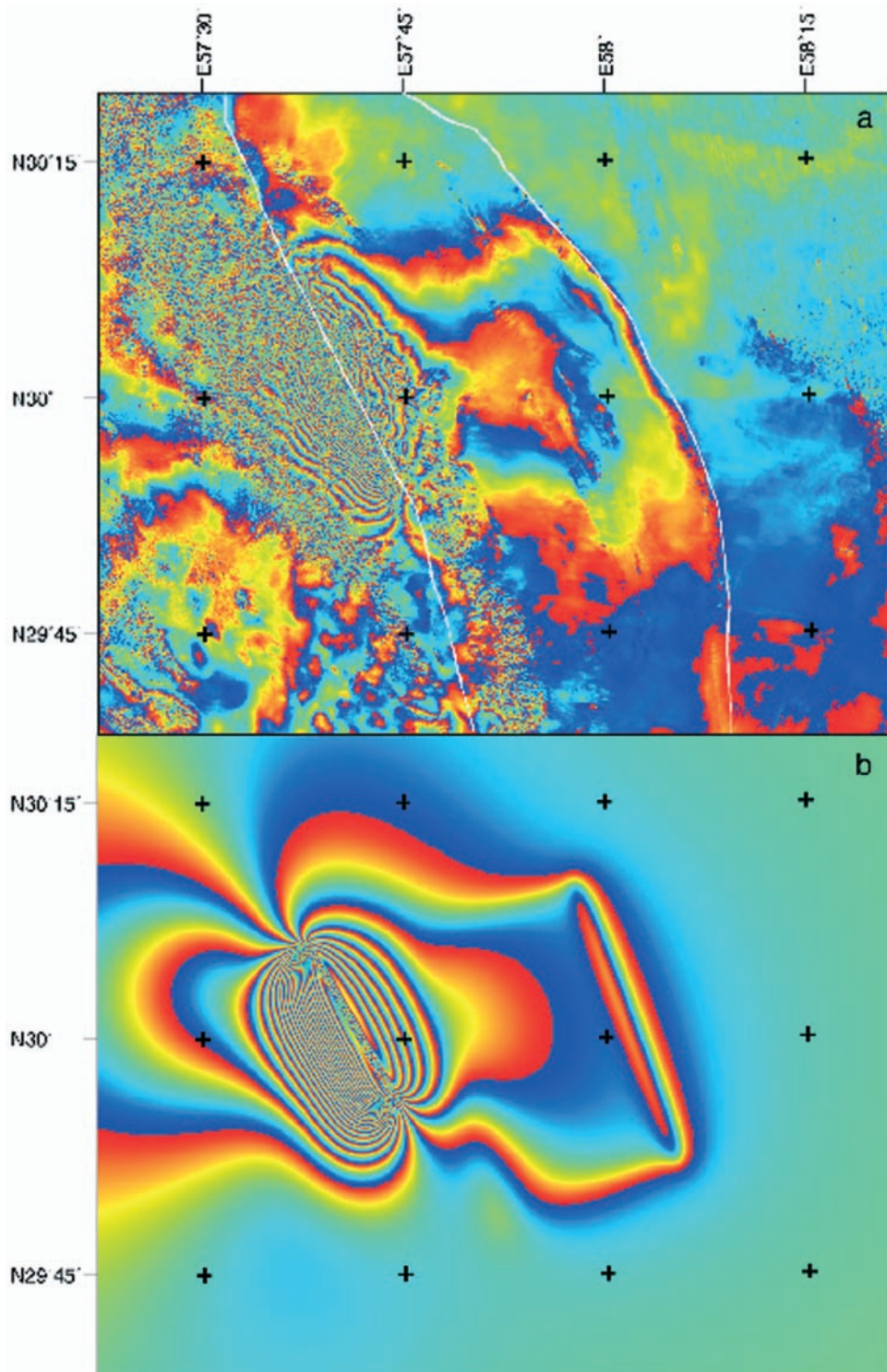


Figure 12. (a) Observed SAR interferogram for the Fandoqa earthquake derived as described in the text. Each colour cycle, from dark blue to red, represents an increase in line-of-sight distance away from the satellite of 28 mm. The white lines are traces of the Gowk fault (west) and Shahdad fault (east). The blotches in the bottom left quadrant of the figure probably represent atmospheric disturbances. (b) Synthetic fringes predicted by an elastic dislocation model with two faults described by the parameters in columns 1 and 4 of Table 3.

The length of the fault rupture is also constrained by the closure of the fringe pattern at the ends of the fault, yielding a value of ~ 20 km, which is close to that observed in the field. The closure is more precise in the south, where the fringes converge nearly at a point, than in the north, where the fringes meet over

a wider zone, indicating that rupture decreases gradually in the north but terminates more abruptly in the south (in contrast to the observations of surface ruptures). In the Gowk valley the fringe pattern is asymmetric, with more fringes on the west side than on the east side. This asymmetry is related to the dip of

the fault, as there will be greater surface displacement in the hanging wall, where a point on the surface at a given distance from the fault is closer to the fault plane than is the corresponding surface point in the footwall. The strike ($\sim 150^\circ$) and dip ($\sim 50^\circ\text{W}$) of the fault estimated from the SAR interferogram agree well with the values obtained from the seismology (Table 3). The wavelength of the fringe pattern either side of the Gowk fault is determined principally by the depth of faulting: the unconstrained SAR inversion result is that faulting extends from the surface to 7 km depth (Fig. 13). The centre of the fault plane should therefore be at ~ 3.5 km depth, which is in reasonable agreement with the seismological centroid determination of 5 ± 2 km. Finally, the sense of the phase shift east of the fault indicates that this side moved towards the satellite, decreasing the line-of-sight distance. Both the vertical (east side up) and strike-slip (right-lateral) components of slip contribute to this effect, leading to a trade-off between the rake on the fault and the amount of slip (and hence moment), with pure strike slip (rake = 180°) requiring greater displacement to match the number of fringes than a rake with a normal component (Table 3). The SAR inversion with all source parameters free (Table 3, column 1) gives a rake with a larger normal component than the seismology (214° compared to 195°) but with a similar moment. Constraining the rake to pure strike slip doubles the moment in the SAR inversion, but does not greatly affect the moment estimate from seismology (Fig. 11, line 3).

In summary, in spite of the trade-off between rake and displacement, the unconstrained SAR inversion gives a result that is consistent with the seismological inversion (Table 3). These inversions are in agreement with most of the field observations also. The only problematic result is that both the SAR

and the seismology suggest a rake with a normal (west-side down) component, whereas a substantial part of the coseismic surface ruptures were downthrown on the eastern side, including the part between Hashtadan and Fandoqa, where observed displacements were largest. We return to this issue later.

3.5 The Shahdad thrusts

The SAR interferogram (Fig. 12a) also shows two fringes east of the Gowk fault, coinciding with an anticline ridge that is assumed to be related to a buried ('blind') thrust at depth, called the Shahdad thrust (Figs 3–6 and 14). This ridge is the easternmost of a subparallel set of curved anticlines (Fig. 9i) in which young (Quaternary?) gravels are deformed by folding and minor thrusting (Fig. 9j) at the surface. They are typically 100–200 m in height, with a half-wavelength of only 2–4 km, suggesting that the thrusts beneath them flatten at depths also of 2–4 km. The SAR fringes associated with the Shahdad thrust can be matched quite simply by a thrust dipping relative to the surface at 8°W beneath the ridges (6°W relative to the horizontal), extending to a depth of only 4.5 km (Fig. 13) and moving only ~ 8 cm (Table 3). Note that the easternmost fringe follows only the central portion of the Shahdad frontal thrust (Figs 12 and 14), showing that displacement on this fault occurred only on the part adjacent to the 1998 Fandoqa rupture in the Gowk valley, but not further north or south. The lateral extent of the fault area that moved is well constrained by the closure of the fringes to the north and south. However, the greater width of the observed fringes on the northern and southern boundaries of the Shahdad thrust (Fig. 12a) compared with the synthetic interferogram (Fig. 12b) suggests that slip varied along the length of the fault rather than being uniform, as we assumed in the modelling. Thus the SAR fringes and the surface geomorphology and geology suggest that a shallow-dipping thrust underlies the ridges bordering the desert east of the Gowk fault. The near-surface sediments in this region are Neogene molasse-like deposits, thought to be at least 3500 m thick, containing well-stratified gypsum-rich marls, sandstones and conglomerates. These sediments probably developed in settings rather similar to those on the western side of the Lut today, where alluvial fans interfinger with salt-rich deposits left by ephemeral lakes. It is easy to imagine that such sediments can produce decollement horizons at shallow depths and Bayasgalan *et al.* (1999) described a similar situation in Mongolia, where thrusts adjacent to strike-slip systems also apparently utilize lake beds as shallow decoupling horizons.

Strictly speaking, we can only say that the inferred movement on the Shahdad thrust system occurred within the May 1996 to September 1998 time interval spanned by the two ERS images used to produce the SAR interferogram. However, we believe that it is probable that the movement occurred during or after the 1998 Fandoqa earthquake. E. Fielding (personal communication) showed that the Shahdad thrust lies in a region where shear stress is expected to have increased as a result of the Fandoqa earthquake. We looked for evidence of movement on the Shahdad thrusts in the 1998 seismograms. However, we were unsuccessful using any realistic set of probable source parameters and it is not difficult to see why. Although the SAR interferogram suggests a substantial moment for the thrust movement (Table 3) it also requires a down-dip width of the thrust of about 20 km. If this moved seismically at a typical rupture velocity of ~ 3 km s^{-1} it would have a time function with a duration

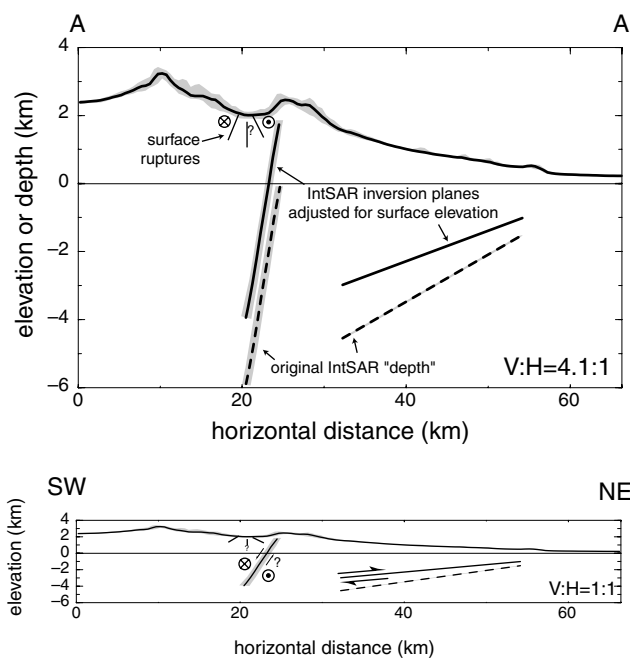


Figure 13. Cross-sections (vertically exaggerated by 4.1 above, true scale below) along the line A–A' in Fig. 3, showing the results of the SAR interferogram inversion (Table 3). The inversion program calculates the position of the dislocation relative to sea level assuming a flat surface, whereas the SAR interferogram measures deformation at the topographic surface. The solid lines show the adjusted positions of the faults (from their original dashed positions) to allow for surface elevation.

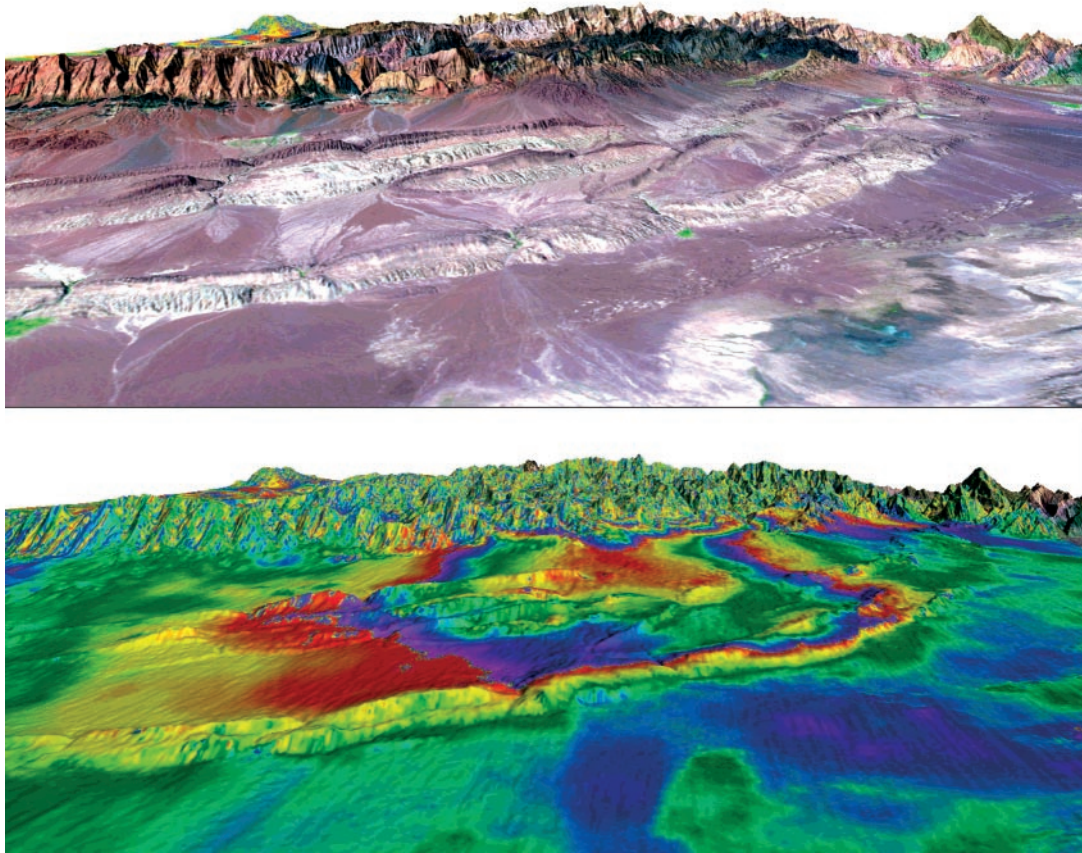


Figure 14. Block perspective views looking west across the anticline ridges above the Shahdad thrust system towards the Abbarik mountains, made by combining digital topography with the LANDSAT TM image. In the lower picture, the SAR interferogram has been draped over the upper image, to show how the edge of the fringe pattern coincides with the frontal ridge. The salt flats of the Dasht-e-Lut are in the foreground.

of about 6 s and the amplitude of the seismograms would be small. This can be seen in line 4 of Fig. 11, where we show such a pulse (with a time function only 4 s long to increase its amplitude) at a time delay after the first motion that corresponds to the second upward pulse seen at NE stations in the main shock (and which we argued earlier was responsible for the later part of the time function in the main seismological inversion of Fig. 10; see also lines 1 and 2 of Fig. 11). We wanted to see whether this later part of the time function could be related to slip on the Shahdad thrust. As can be seen in line 4 of Fig. 11, such slip produces the wrong polarity for P waves at those NE stations (e.g. YAK). It also causes a pulse that is not seen at southern stations (e.g. LBTB), despite them being particularly sensitive as they are close to the null (B) axis for the main strike-slip event but close to the T -axis for the thrust. The SH waves are too small in amplitude to be detected amidst the much larger SH waves from the strike-slip fault. The second upward P pulse at NE stations (YAK) can only be produced by a compressional onset, which requires a steeper dip of at least 40° if it is to be caused by a thrust (shown in line 5 of Fig. 11). However, there is no evidence for this in the SAR interferometry and it produces pulses that are not seen in the observed seismograms at southern stations (e.g. LBTB in line 5, Fig. 11).

Thus, although there is no direct evidence that the Shahdad thrust system slipped seismically during the Fandoqa main shock, we cannot rule it out, because the effect on the seismograms may have been too small to be observed. However, we suspect

the slip was in fact aseismic or occurred at low rupture velocities, mainly because the ratio (α) of displacement to length on the Shahdad thrust determined by SAR interferometry is very small ($\sim 2 \times 10^{-6}$) and far less than the value of $\sim 5 \times 10^{-5}$ that is typically seen on seismogenic ruptures (e.g. Scholz *et al.* 1986). For comparison, the value of α for the Fandoqa strike-slip fault is $\sim 6 \times 10^{-5}$ (Table 3). The ratio α is related to the elastic strain released by fault rupture and seismogenic faults are expected to be able to accumulate more than was seen to have been released by the Shahdad thrust (e.g. Scholz *et al.* 1986). Note, however, that we assumed the deformation above the thrust was elastic in deriving a fault model for the Shahdad thrust from the SAR fringes.

3.6 Summary

In summary, the seismology, SAR interferometry and surface observations provide a consistent and relatively simple image of the strike-slip movement on the Gowk fault during the 1998 Fandoqa earthquake (Table 3), with an average displacement of about 1.3 m on a fault about 21–23 km long, extending from the surface to a depth of about 7 km (Fig. 13). Both the seismology and SAR require the fault to dip west at about 50° – 55° . The main uncertainty is in the vertical component of motion: the SAR and seismological data suggest a normal component of 0.3–0.8 m down to the west, whereas the surface ruptures show displacements down to both west and east, with

the greatest offsets on scarps down to the east. The nature and significance of this vertical component concern the tectonics of the Gowk fault zone as a whole and its relation to the Shahdad thrusts, so we return to this question after having reviewed the evidence from the other major earthquakes on this system since 1981.

In addition to the coseismic slip on the Gowk fault, the SAR interferometry reveals about 8 cm of slip on a parallel thrust about 30 km to the east. The timing of the ERS images used to make the interferogram make it likely that slip on the thrust was triggered by the Fandoqa earthquake, but we suspect that it occurred aseismically.

4 SURFACE FAULTING IN THE 1998 NOVEMBER 18 CHAHAR FARSAKH EARTHQUAKE (M_w 5.4)

On November 18 1998, eight months after the Fandoqa earthquake, a smaller event of M_w 5.4 affected the northern end of the Gowk fault system near Chahar Farsakh (Figs 5 and 15). Damage was localized to houses at Chahar Farsakh (VI+), the Emamzadeh Zeid mausoleum and Puzeh Bagh (VI+), and the shock was felt strongly at Hashtadan (V), Fandoqa (IV) and Golbaf (IV). This earthquake produced some surface ruptures noted the following day by Mr Rowshan Ravan (GSI Director, Kerman Office) and still visible when visited by some of the present authors (MB, MQ, JJ, MT) in April 1999. The ruptures were small, discontinuous open cracks and fissures of only a few centimetres in offset but approximately 4 km in total length (Fig. 15) and followed precisely the ruptures observed after the 1981 Sirch earthquake, which had also been observed by the same people (MB, MQ). Near Chahar Farsakh itself the 1981 ruptures were similarly small fractures, but further north near the Shahdad river (Fig. 15) the minor 1998 ruptures followed a scarp on which the largest right-lateral strike-slip displacement (43 cm) was observed in 1981 (Fig. 8).

The 1998 November 18 earthquake was too small for us to use the long-period P and SH waves to constrain its mechanism and depth, but the Harvard CMT solution (Table 1, Fig. 3) shows nearly pure right-lateral strike-slip on a N–S fault, consistent with slip on the branch of the Gowk fault through Chahar Farsakh. It is difficult to prove that the minor fractures in 1998 represent true reactivation of the Gowk fault rather than consolidation of near-surface deposits, especially since an earthquake of M_w 5.4 is only expected to produce a slip of the order of 20 cm on a fault of dimension about 4×4 km (assuming an equidimensional fault plane with a slip-to-length ratio of 5×10^{-5}), and rupture may not have reached the surface if the hypocentre was deeper than about 5 km.

The Gowk fault at Chahar Farsakh has a vertical component of motion, responsible for uplifted terraces of the Shahdad river on its western side, on which Chahar Farsakh and Emamzadeh Zeid mausoleum are built at heights of ~ 60 and ~ 20 m above the Shahdad playa respectively (Fig. 16). Travertines that appear to drape the terrace riser at Chahar Farsakh (Fig. 16) may allow the future dating of offsets on the fault. There is little in the local geology or geomorphology to indicate whether the vertical component involves shortening or extension. The Harvard CMT solution for the 1998 November 18 earthquake shows a dip of 55° W for the N–S right-lateral nodal plane, as was found also for the 1998 Fandoqa main shock. If this earthquake really was on the Chahar Farsakh branch of the

Gowk fault it would suggest a long-term reverse (shortening) component on that fault (although the earthquake itself was apparently almost pure strike slip). However, the fault at Chahar Farsakh is strongly curved in plan view, with a strike of 160° in the north and 195° in the south (Fig. 15). At its northern end it appears to merge with thrusts, but an overall N–S slip vector (as seen in the CMT solution for the 1998 November 18 earthquake; Table 1) could produce an extensional component at Chahar Farsakh and the Shahdad river. Once again, a definitive interpretation of the vertical component of slip seems elusive.

5 THE 1981 JUNE 11 GOLBAF EARTHQUAKE (M_w 6.6) REVISITED

The 11 June 1981 Golbaf earthquake produced surface ruptures on two subparallel N–S strands of the Gowk fault system, 14.5 and 7.5 km long, SE of Golbaf (Figs 5 and 8). Displacements were small, typically with 3 cm right-lateral strike-slip and 5 cm vertical offset (E side up) on the longer eastern fault and hairline cracks on the shorter western one (Berberian *et al.* 1984). Early analysis of the P waveforms, with only limited forward modelling, was sufficient to show that the rupture was complicated, involving slip in at least two subevents of different orientations (Berberian *et al.* 1984). This analysis probably explains why the Harvard CMT solution had a large non-double-couple component (Table 1), but could not provide strong constraints on the source processes involved. We analysed the waveforms again, using SH as well as P , and again found that two subevents were needed to match the observed seismograms (Fig. 17). The orientation of the first subevent is well constrained by the P and SH first motions (see also Berberian *et al.* 1984), and requires a N–S right-lateral nodal plane to be dipping west at $\sim 50^\circ$, as at Fandoqa (1988 March 14) and Chahar Farsakh (1998 November 18). In this case, the E–W nodal plane, which is presumably the auxiliary plane, is tightly constrained by first motions and must dip steeply north, requiring a minor reverse component on the right-lateral plane (a rake of 156°).

However, the observed seismograms cannot be matched with a single source in the orientation constrained by first motions, as shown in lines 2, 4 and 5 of Fig. 18. A single source at 20 km depth (line 2) can match the inflection in P waves to the south (NAI) but not the double-upward pulse to the north (KON). A single source at 10 km (line 5) can match the double pulse at KON but not the inflection at NAI. Line 4 shows the results of an inversion with the mechanism constrained to the orientation and depth of the Harvard CMT solution, which fails to match stations to the east (GUA). In all three cases the fit to the SH waves is bad. A much better fit (line 1 and Fig. 17) is achieved when a second subevent is included 2.2 s after the first and offset 8 km to the west. The offset in time and space between the two subevents is necessary to fit both the double pulses to the north (e.g. KON) and the relatively simple pulses to the south (e.g. NAI), but the main effect of the second subevent is to improve the fit of the SH waves, as the almost pure strike-slip mechanism with vertical nodal planes produces relatively small P waves (line 3). After many trial-and-error tests, our best result was obtained with a first source at about 20 km depth [which was also the depth obtained by Harvard and by Berberian *et al.* (1984)], but neither this nor the orientation of the second subevent is well constrained.

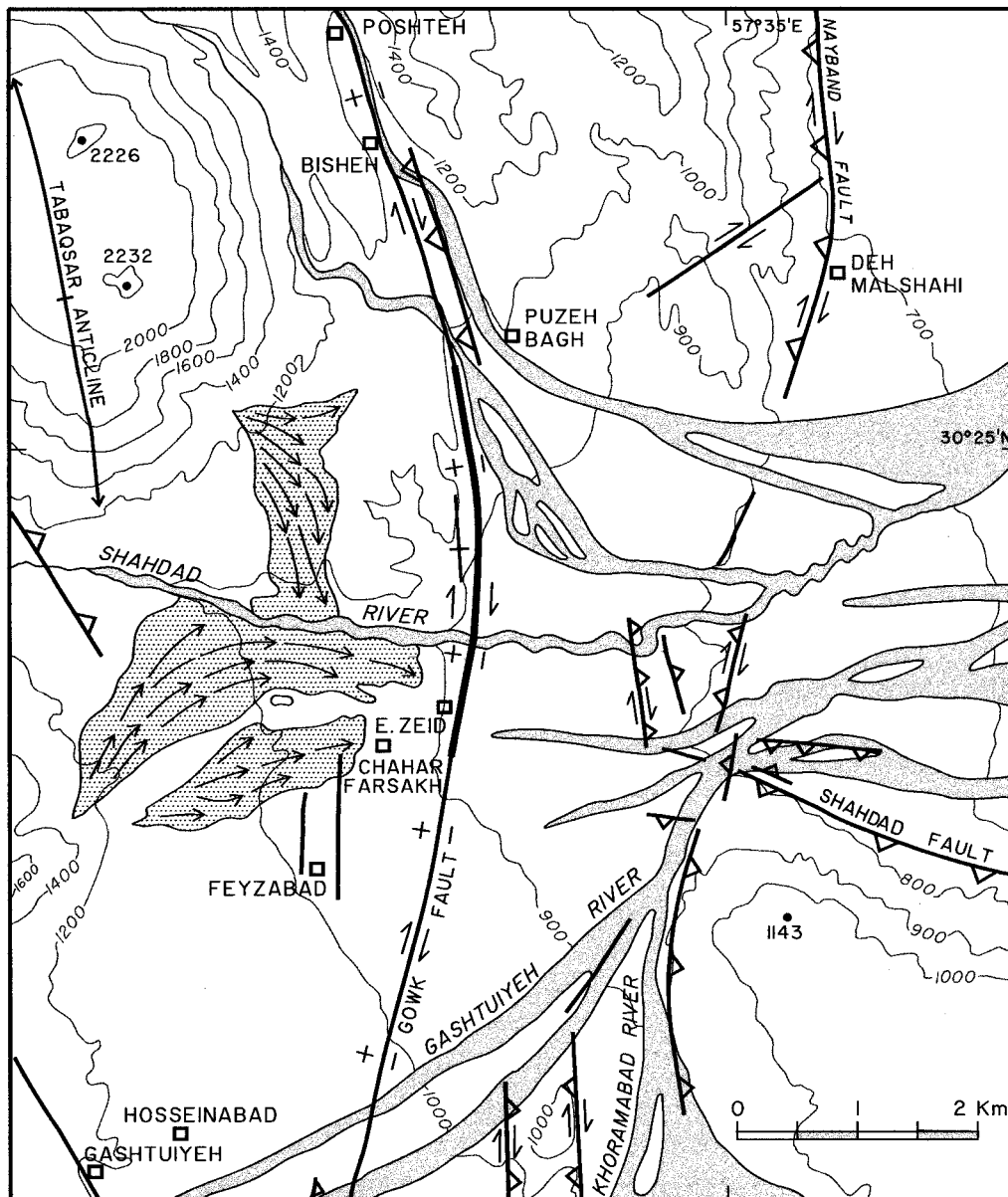


Figure 15. Detailed map of the northern end of the Gowk fault zone, including the area affected by the 1998 November 18 earthquake near Chahar Farsakh (M_w 5.3) and the location of surface cracks observed after that earthquake (thick line). The stippled regions with arrows are old fans and their flow directions, now abandoned by the deep incision of the Shahdad river through the uplifted (west) side of the Gowk fault. Except for the Nayband fault, the transverse fault W of Deh Malshahi, the Shahdad fault and the fault SW of the Tabasqar anticline, all other faults were reactivated at the surface during the 1981 July 28 Sirch earthquake (M_w 7.1).

Nonetheless, a centroid depth of ~ 20 km makes some sense in this case. Only ~ 3 cm of right-lateral strike-slip motion was observed at the surface after this earthquake, whereas from the estimated seismic moment of about 4×10^{18} N m (the same value for both the Harvard solution and our first subevent) we might expect a slip of about 75 cm on a fault with dimension ~ 15 km, assuming an equidimensional fault with a slip-to-length ratio of 5×10^{-5} . This dimension agrees with the rupture length observed on the more substantial eastern strand of the surface ruptures, but the observed displacements were far too small. With a centroid of 10–15 km or deeper, however, it is likely that most of the slip failed to reach the surface.

6 THE 1981 JULY 28 SIRCH EARTHQUAKE (M_w 7.1) REVISITED

The 28 July 1981 Sirch earthquake produced 65 km of discontinuous surface ruptures on both sides of the Gowk valley from Zamanabad to the north of Chahar Farsakh (Figs 5, 8 and 19 and Berberian *et al.* 1984). These ruptures were anomalous in that the maximum measured displacements were less than 50 cm (right-lateral and vertical) and displacements on most ruptures were much less than this (Fig. 19a). With a typical slip-to-displacement ratio of 5×10^{-5} , a fault with this length might be expected to move about 3.3 m. Consideration of the

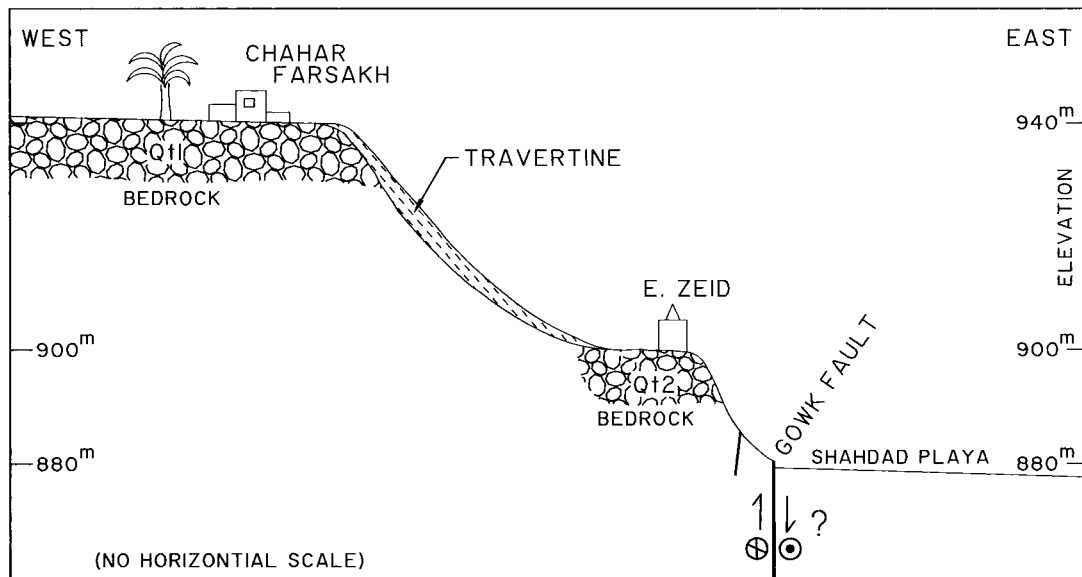


Figure 16. E–W cross-section through Chahar Farsakh, showing two uplifted terraces of the Shahdad river west of the Gowk fault, and the recent travertine deposit that drapes them. The attitude of the Gowk fault at depth, and whether it has a reverse or normal component at this location, are not known, so it has been drawn as vertical (see text).

seismic moment, which was between 4×10^{19} and 9×10^{19} N m (Table 1), equivalent to $\sim M_w$ 7.1, leads to the same conclusion. Such an earthquake usually breaks the entire seismogenic thickness of the upper crust, typically about 15 km. Taking this value as the down-dip width of the fault, and again a slip-to-displacement ratio of 5×10^{-5} , we would expect a fault length of 42–63 km and an offset of 2.1–3.2 m. As for the earlier Golbaf earthquake, we conclude that the observed fault length is roughly that expected but the observed surface displacements were apparently too small.

The body wave seismograms for the Sirch earthquake are complicated and many WWSSN seismograms were off-scale, so that fewer are available than for the earlier Golbaf earthquake. Forward modelling of long-period P waves, long-period first motions and analysis of a single strong-motion recording at Golbaf by Berberian *et al.* (1984) was sufficient to show that the earthquake was a multiple event lasting about 40 s, beginning with a small event that must have a large thrust component followed by at least three other subevents that were much bigger. The main moment release begins about 12 s after the first motions.

The Harvard CMT solution for this event has a smaller non-double component than for the earlier Golbaf earthquake (Table 1). The best double-couple source is a shallow-dipping (13° W) thrust with a strike of 150° , nearly parallel to the Gowk fault, and a rake with a small right-lateral component (119°). Using the available long-period P and SH waveforms, we carried out an inversion in which the source orientation was fixed to that of the Harvard best double-couple solution, but the time function and depth were free (Fig. 20a). Since the time function duration is 40 s or more we used time function elements of half-duration $\tau=4$ s, so we can not expect to match the shorter-wavelength features of the seismograms. This Harvard solution reproduces the general shapes and polarities of the SH waveforms, including the small amplitudes at nodal stations to the south (SLR and GRM). It is less successful with the

P waveforms. In particular, P waves at stations to the east and NW have significant amplitudes but cannot be matched by this solution since those stations are close to the steep nodal plane. The fit at stations to the south (GRM, NAI), which are away from nodal planes, is much better. Furthermore, this solution violates several compressional long-period P -wave first motions to the north and east (see also Berberian *et al.* 1984). None of this is surprising: (1) the earlier analysis of Berberian *et al.* (1984) showed the earthquake to be a multiple event; (2) the amplitude of the first 10 s of the P seismograms is so small compared to the later part of the records that the moment of the first subevent is clearly minor; (3) the strong P signals at stations in nodal positions on the focal sphere indicate that the source orientation in Fig. 20a cannot alone account for what happened. The Harvard CMT inversion, in which the observed seismograms are low-pass filtered at 45 s, can only hope to provide some average of the overall rupture process.

Fig. 20(b) shows a second inversion, in which all source parameters were free to change, obtained using the solution in Fig. 20(a) as a starting position. The solution in Fig. 20(b) provides a better fit to the P waves in the NW (although not to the E) without degrading the fit to SH waveforms at most stations. In terms of the fit to the data, the solution in Fig. 20(b) is marginally better than in Fig. 20(a), with a drop in residual of 10 per cent. However, we do not believe it is significantly better; most parameters are not well resolved. In numerous tests we found that some right-lateral strike-slip on a roughly N–S nodal plane was needed to improve the fit to the P waves without destroying the fit to SH waves. The reason for this is clear from the earlier Golbaf event (Fig. 17), where the SH waves have similar nodal planes in both solutions. We experimented with using an additional subevent to improve the fit of P waves at eastern stations, and some improvement is possible, but the resulting source models are not well constrained. With such limited data there is little more we can do. In principle, the Harvard CMT solution should give the best

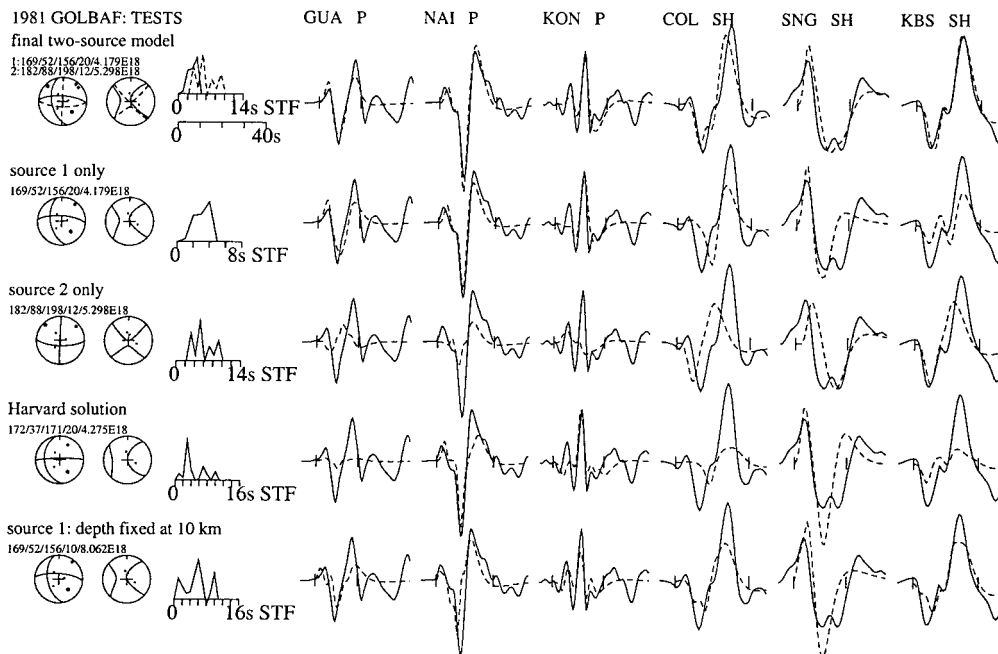


Figure 18. Tests to investigate the sensitivity of the 1981 Golbaf earthquake seismograms to various source parameters (see text). The layout is the same as in Fig. 11. The first line shows selected seismograms from the solution in Fig. 17. Lines 2 and 3 are forward models showing the contribution of the first (line 2) and second (line 3) subevents to the synthetic seismograms. Line 4 shows the result of an inversion in which the strike, dip and rake are fixed to the values of the Harvard CMT ‘best-double-couple’ solution, while other parameters are free to change. Line 5 shows the result of a single-source inversion in which the strike, dip and rake fixed to the values of the first subevent in line 1, but with the depth fixed at 10 km (see text).

arguments as before, an event of this size might be expected to occur on a fault ~ 8 km long that slipped ~ 0.4 m. However, the depth is not well constrained by the seismic data, and whether the small surface ruptures can be attributed to a deeper centroid or to the unconsolidated playa deposits in which most of the ruptures were seen remains uncertain.

8 REPETITION OF EARTHQUAKES ON THE GOWK FAULT SYSTEM?

Between June 1981 and December 1998 five earthquakes occurred that were associated with observed surface ruptures

on the Gowk fault system. Ruptures in the last three earthquakes of this sequence, in November 1989 (M_w 5.8), March 1998 (M_w 6.6) and November 1998 (M_w 5.4), precisely followed shorter portions (~ 10 , 20 and 4 km respectively) of the much longer surface ruptures that formed in June and July 1981 (14 km and 65 km respectively). There is little doubt that the surface ruptures coincided in these earthquakes, as they were mapped in the field by the same people (MB and MQ) each time. It can be argued that the two smallest events of the sequence in November 1989 (M_w 5.8) and November 1998 (M_w 5.4) were too small to be unequivocally associated with rupture at depth on the faults whose surface reactivation showed only minor cracking, and that those surface cracks may

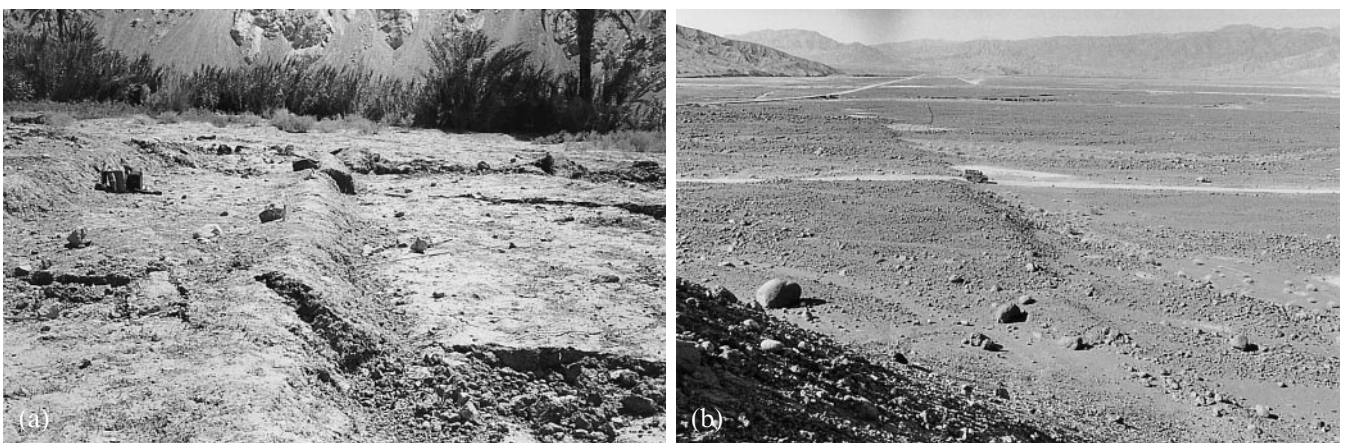


Figure 19. Two views of the co-seismic faulting in the 1981 Sirch earthquake. (a) Two parallel ruptures, each with right-lateral offsets of ~ 10 – 15 cm, 10 km north of Chahar Farsakh, looking east. These were typical of the largest offsets seen in 1981, and are far smaller than the maximum coseismic offsets of ~ 300 cm seen after the Fandoqa earthquake in 1998. (b) View south near the Shahdad river about 1 km east of Chahar Farsakh. The 1981 scarp, up on the eastern side, is by the vehicle.

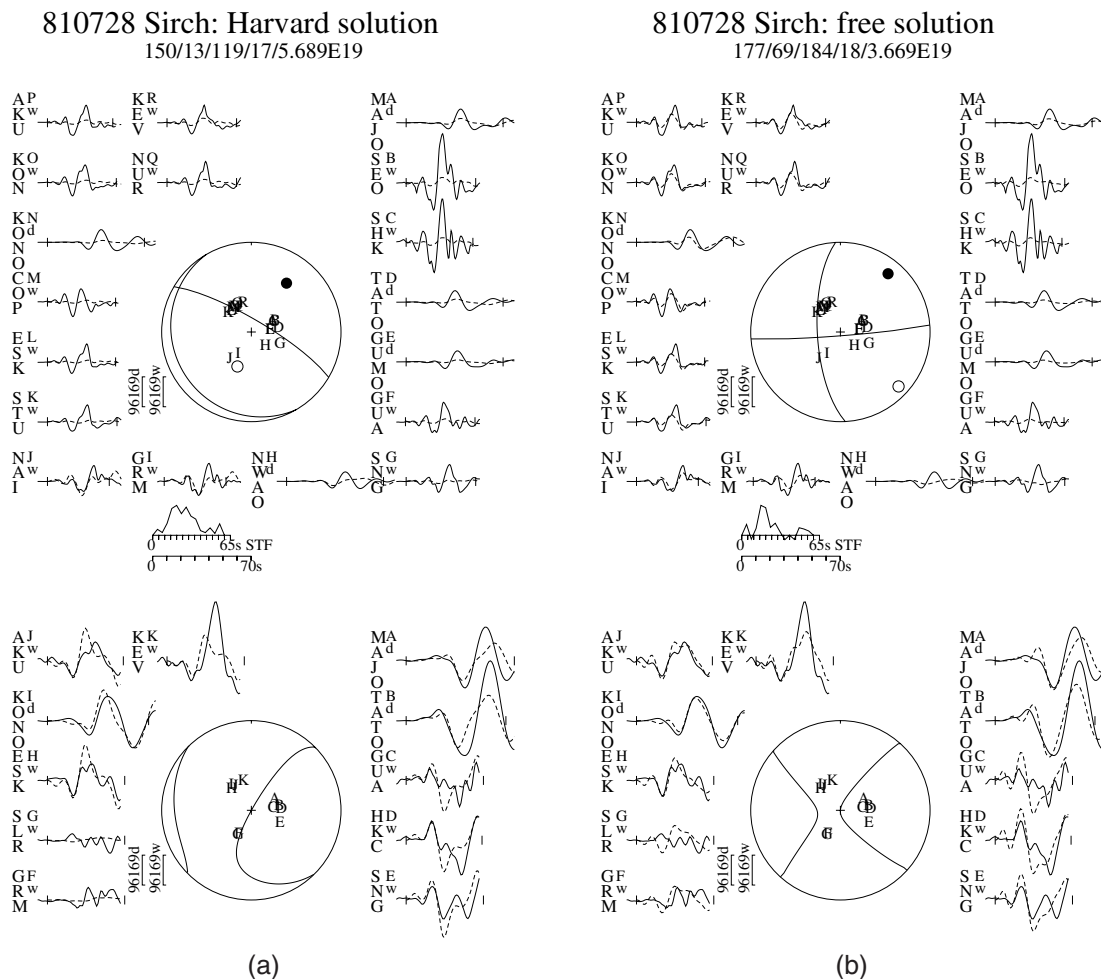


Figure 20. Observed and synthetic seismograms for the 1981 July 28 Sirch earthquake (Table 1). Layout and conventions are the same as in Figs 10 and 17. (a) An inversion with the strike, dip and rake fixed to values from the Harvard CMT ‘best double-couple’ solution. (b) An inversion with all parameters free, using a single source.

represent unimportant local effects related to ground shaking or compaction of unconsolidated sediments. It is more difficult to argue along those lines for the coincidence between the surface ruptures in the 1981 July 28 Sirch (M_w 7.1) and the 1998 March 14 Fandoqa (M_w 6.6) earthquakes. Although the ruptures in the 1981 Sirch event were anomalously small for its size, they were regular, with consistent right-lateral offsets of up to 40 cm, although these were more typically 10 cm where they coincided with the later March 1998 faulting. It is difficult to see how regular strike-slip offsets of this amplitude can occur by shaking or consolidation effects. At least for the 1981 July 28 (Sirch) and 1998 March 14 (Fandoqa) earthquakes, it seems certain that coseismic surface rupture occurred twice in the same place within 17 years.

This sequence therefore raises two main questions.

(i) Why did the 1981 Golbaf (M_w 6.6) and Sirch (M_w 7.1) earthquakes produce surface offsets much smaller than expected from their seismic moments, even though the length of those ruptures was approximately as expected?

(ii) Why did the smaller (M_w 6.6) 1998 Fandoqa earthquake produce much larger (up to 3 m) surface offsets than the substantially bigger (M_w 7.1) 1981 Sirch earthquake (up to 0.4 m) on apparently the same fault?

We can think of three possible answers to these questions. The ‘expected’ surface offset depends entirely on the expected ratio (α) of displacement to length on the faults. For intracontinental earthquakes this value is typically 5×10^{-5} and varies by less than an order of magnitude (Scholz *et al.* 1986). This ratio is related to the static stress drop on the fault, and is equivalent to saying that stress drops are typically between 1 and 10 MPa (10–100 bar). If α were substantially less than the typical value, presumably representing some special property of the Gowk fault, this could explain the low displacement in the Golbaf and Sirch earthquakes. However, the value of α for the 1998 March 14 Fandoqa earthquake is $\sim 6 \times 10^{-5}$, conforming closely to the global pattern, and this occurred *on the same fault*. It is therefore difficult to argue that the Gowk fault has any intrinsically special mechanical properties.

A second possibility is that the ruptures in 1981 were small because they occurred in soft unconsolidated sediments, or that rupture failed to reach the surface because of decoupling horizons at shallow depth. This explanation is also implausible because the 1998 Fandoqa earthquake produced substantial surface offsets, fully consistent in length and amplitude with that expected from the global scaling relations, *in the same place* as where fault slip was apparently missing in the 1981 Sirch earthquake.

891120 South Golbaf Mw 5.8

145/69/188/10/7.03E17

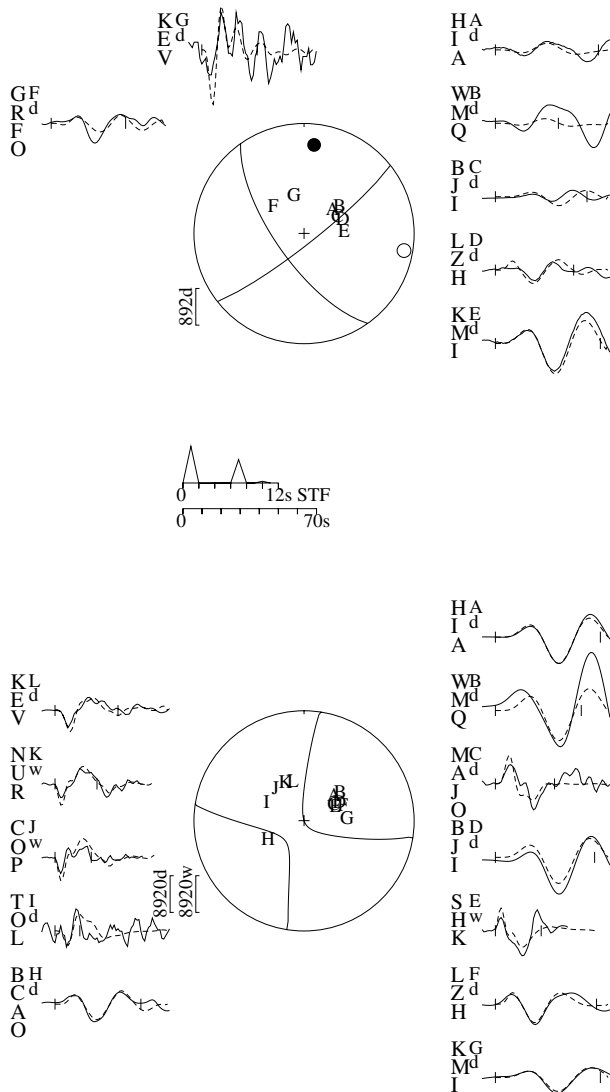


Figure 21. Observed and synthetic seismograms for the 1989 November 20 South Golbaf earthquake (Table 1). Layout and conventions are the same as in Figs 10 and 17.

A third possibility is that rupture in the 1981 earthquakes occurred deeper than in the 1998 Fandoqa event, and that only minor displacement reached the surface. This explanation is consistent with the centroid depths of ~ 20 km found in our waveform inversions for the first subevent in June 1981 (Fig. 17) and for the 1981 July Sirch earthquake (Fig. 20), although these were both complicated multiple-event earthquakes and we cannot claim that those depths are well resolved. These depths contrast with the much shallower centroid (5 ± 2 km) for the 1998 Fandoqa earthquake, which is well-resolved by both seismology and SAR interferometry. The attraction of this explanation is that it is not necessary to appeal to any special effects: the 1981 earthquakes simply ruptured deeper parts

(perhaps depths of 5–15 km) of a fault system that later broke at shallower depths (0–7 km at Fandoqa in 1998, and possibly also at shallower depths at Chahar Farsakh in November 1998 and South Golbaf in 1989). In addition, if the 1981 earthquake ruptured principally on a shallow-dipping thrust (the Harvard solution), little of this slip might be expected at the surface and the strike-slip displacement that was seen might relate to a smaller subevent (although this would not explain the anomalous slip-to-length ratio). It seems to us that a greater depth, possibly combined with a shallower-angle dip in the July Sirch earthquake, is the most likely explanation for the relatively small ruptures in 1981 compared to those in 1998. We return to the significance of this conclusion later.

Finally, it is worth performing a small thought experiment. The 1998 Fandoqa ruptures follow clear pre-existing fault scarps along their entire length. Trenches excavated across these scarps at some future date would reveal two offsets, corresponding to the earthquakes of 1981 and 1998, with the 1981 offset much the smaller of the two. A reasonable conclusion would be that the magnitude of the 1981 event was also the smaller of the two, but that is precisely wrong: it was much bigger. It is difficult to see how evidence from trenching could reveal the quite different characteristics of those two earthquakes. Conversely, future historians researching the damage distributions of the two earthquakes would rightly conclude that the 1981 event was much bigger, having been felt over a much wider region, but they could not deduce the very different characteristics of the ground ruptures in the two events. There are salutary lessons in this sequence of earthquakes for those attempting to assess seismic hazard or the tectonic significance of earthquakes from trenching or historical records alone.

9 ACTIVE TECTONICS OF THE GOWK-SHAHDAD FAULT SYSTEM

Two important tectonic questions arise from the 1981–1998 earthquake sequence on the Gowk fault system:

(i) What are the relations between the strike-slip motion on the Gowk fault, the thrusts at Shahdad and the regional tectonics?

(ii) What is the nature and significance of the vertical component of motion on the Gowk fault? This question arises from a number of apparent contradictions. The surface ruptures in 1998 were both W- and E-side down, with the largest offsets E-side down, whereas the seismology and SAR interferometry indicate a normal component on a west-dipping fault (i.e. W-side down). Meanwhile, the first subevents in both 1981 earthquakes involved a reverse component on the west-dipping right-lateral nodal plane.

Help in answering these questions comes from consideration of the regional tectonics and local geomorphology. The Gowk fault is part of a longer right-lateral strike-slip system that borders the western side of the Dasht-e-Lut (Figs 2, 3 and 6). To the north, the Nayband fault continues for at least 200 km beyond Chahar Farsakh as an almost straight line. Strike-slip faulting also continues for 200 km beyond the southern terminus of the Gowk fault on the Sabzevaran fault (Fig. 2), which is 30 km west of the Gowk fault and separated from it by the mountains of the Jebel Barez magmatic arc. Both the Nayband and Sabzevaran faults strike $\sim 175^\circ$ and, except near their junctions with the Gowk fault, they are not associated

with much topographic relief. From this we deduce that the regional slip vector on the system is also approximately 175° . By contrast, the Gowk fault strikes $\sim 155^\circ$ and is associated with substantial topographic relief (Figs 3 and 4), both between the Kerman plateau and the Dasht-e-Lut (~ 2000 m) and between the Gowk valley and the ranges to either side (~ 1000 m). From this evidence we expect the Gowk fault system to involve an overall component of shortening.

By far the best-constrained earthquake slip vector on the Gowk fault comes from the 1998 Fandoqa event. The other earthquakes are either small with mechanisms that are not well constrained (1989 south Golbaf and 1998 Chahar Farsakh) or complicated multiple events (1981 Golbaf and Sirch). The 1998 Fandoqa slip vector is 147° , roughly parallel to the Gowk fault and $\sim 30^\circ$ anticlockwise from the expected overall slip vector of 175° . If this is representative of the Gowk fault, then the shortening component must be taken up elsewhere, and the obvious place is on the Shahdad thrusts. The SAR interferometry indicates almost pure thrust motion on the Shahdad fault, with a slip vector of $\sim 062^\circ$, which is nearly perpendicular to the slip vector in the 1998 Fandoqa earthquake. This situation clearly resembles the spatial separation of strike-slip and shortening components of oblique convergence that is so common in oceanic subduction zones and is commonly known as 'partitioning' (e.g. Fitch 1972; McCaffrey 1992). Before considering how this separation is achieved on the Gowk and Shahdad system, we must examine geomorphological constraints on acceptable fault geometries.

The valley followed by the Gowk fault is characterized by several deep depressions, such as those at Hashtadan, Fandoqa, Golbaf and South Golbaf (Fig. 6). These basins are filled with sediment derived from rivers draining the mountains to the west. Some of these basins (Hashtadan, Golbaf) also have exits, draining through deep gorges in the mountains east of the Gowk valley to the Shahdad plain. Others (such as Fandoqa)

are now internally draining, but are near uplifted dry valleys on their eastern side that were once occupied by rivers draining through to the Lut. Late Quaternary fault scarps in the Gowk valley also show a regular pattern in which the flanks of the valley are uplifted and the middle is downthrown. These observations all suggest that the base level of the Gowk valley is generally being lowered relative to the mountains on the east. The rivers flowing through the anticlines of the Shahdad thrust system also cut deep gorges through the rising ridges, so that the area between these ridges and the Gowk fault is also being uplifted relative to the Shahdad plain. The lowest elevation of the Gowk fault itself is at its northern end near Chahar Farsakh. This is the only place where it is in direct proximity to the Shahdad plain (Fig. 19b), but here the end of the Gowk fault is in a clear pull-apart relation with the southern end of the Nayband fault, probably accounting for the deep local depression in this location. It may be this local subsidence that has caused the incision of the Shahdad river near Chahar Farsakh and attracted the streams draining round the ends of the Nayband and Shahdad faults (Fig. 15).

We can now consider fault geometries that achieve slip 'partitioning' by separating oblique slip at depth into its strike-slip and thrust components near the surface and that are also consistent with the available evidence. The simplest configuration, found in some island arcs, is illustrated in Fig. 22(a). It is stable because the slip vector on the strike-slip fault (AC) lies within the underlying thrust plane, which is co-planar (i.e. BC and AB have the same dip), and can accommodate large finite slip on the faults. Fig. 13 shows the configuration of the 1998 Fandoqa earthquake fault and the Shahdad thrust determined from the SAR interferogram. A down-dip projection of the Shahdad thrust meets the Fandoqa (Gowk) fault at a depth of about 6 km, well within the seismogenic crustal thickness. From the previous discussion (Section 8) we expect that the 1981 Sirch earthquake occurred principally on a fault

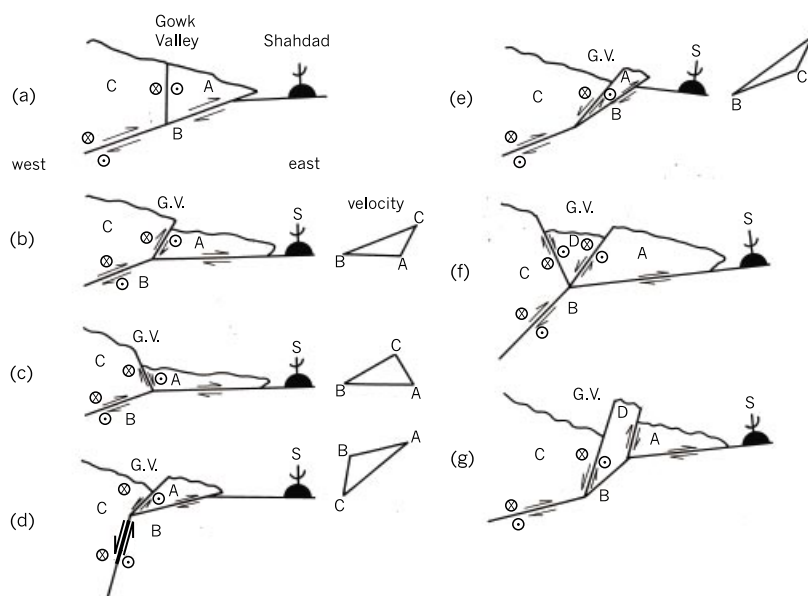


Figure 22. E–W cartoon cross-sections to illustrate possible fault geometries in and beneath the Gowk valley and Shahdad thrust system (see text). Velocity triangles to the right of cartoons (b) to (e) illustrate the relative motions of fault-bounded blocks A–C. In the text, faults are referred to by the blocks they bound; thus 'fault AB' is the fault bounding blocks A and B.

below this intersection. Recalling that the Shahdad thrust has a dip of $\sim 6^\circ$ (Table 3) and that the best double-couple Harvard CMT solution for the 1981 Sirch earthquake had a nodal plane dipping 13° W (Table 1), it is just possible that the overall geometry resembles that in Fig. 22(a) and that faults AB and BC could be roughly co-planar. However, this configuration would not require any vertical motion on the Gowk fault (AC), whereas the late Quaternary fault scarps and the geomorphology all suggest that the middle of the Gowk valley is systematically lowered relative to the mountains on the eastern side.

A vertical component of motion on fault AC is required if AB and BC have different dips. If BC is steeper than AB, as suggested by our inversions for the 1981 Golbaf (Fig. 17) and Sirch earthquakes (Fig. 20b), then the motion on AC would have a reverse component if it dips west (Fig. 22b) or a normal component if it dips east (Fig. 22c). Neither of these match the seismological and SAR data for the 1998 Fandoqa earthquake, which evidently requires a normal component on a west-dipping fault. A normal component on a west-dipping fault is compatible with either a normal component at depth on BC (Fig. 22d), for which there is no evidence, or with a thrust component at depth on BC, but only if BC has a more shallow dip than AB (Fig. 22e), which is not likely given that AB only dips at 6° anyway. At this point we should realize that none of the configurations in Fig. 22(b)–(e) is stable, as any vertical component on fault AC means that its slip vector does not lie in the direction of the intersection where the fault planes meet. None of these configurations can therefore accommodate finite motion on the system anyway. In these circumstances it is very likely that more than one fault will be required at shallow levels in the Gowk valley. The problem is then unconstrained and several configurations are possible. One example is shown in Fig. 22(f), in which extension in the hanging walls of the faults bounding block B is taken up by two faults (CD and AD), both with a normal components, that dip towards each other to create a graben floored by block D. This does not seem a likely configuration to us as there is no evidence of substantial east-facing faulting on the western side of the Gowk valley north of Golbaf; the dominant faulting is all on the eastern side. Another alternative is shown in Fig. 22(g), in which the Shahdad fault does not continue west at constant 6° dip to join the 1998 Fandoqa fault, but instead steepens beneath the Abbarik mountains east of the Gowk valley to form a ‘ramp-and-flat’ configuration at depth. This would give the geometry of Fig. 22(e) beneath the Gowk valley, allowing west-dipping normal faulting, presumably matched by thrust faulting on the eastern side of the mountains. The geometry in Fig. 22(g) (and in Fig. 22f) is clearly unstable. Some complicated deformation must occur where faults meet to overcome space problems and the faulting should evolve with time. However, the configuration in Fig. 22(g) is at least compatible with the observed slip on the Shahdad fault (AB), the Fandoqa fault (AD), our suggestion for the deeper ruptures in the 1981 Golbaf and Sirch earthquakes (oblique thrust fault BC, either steep or shallow-dipping), the overall geomorphology of the Gowk Valley and with the sense of vertical motion on Late Quaternary faults in the Gowk valley.

An apparent difficulty with Fig. 22g is reconciling it with the observed sense of the vertical motions on the surface ruptures in 1981 and 1998. In 1998, substantial vertical motions of ~ 1 m down to the *east* (in the opposite sense to those inferred from

SAR interferometry and seismology) were observed on the linear scarps 5 km south of Hashtadan and 2–3 km south of Fandoqa (Figs 7, 8 and 9d). Since both places are at right-stepping breaks in the overall faulting, it is possible that some of this vertical component was related to a pull-apart effect that dropped the central valley floor. In both places faults occur to the east of the surface ruptures that were not apparently reactivated in 1998. Furthermore, in both places the east-facing scarps were in unconsolidated fan material deposited in long stream systems draining the Sekonj mountains to the west of the Gowk valley. We suspect that the east-facing scarps represent a steep, local, tensional failure within the fan material adjacent to the faulting that bounds the eastern side of the valley. This phenomenon is sufficiently localized to not affect the overall lowering of the Gowk valley relative to its eastern side observed by the SAR interferogram. In other places, particularly in the Hashtadan, Fandoqa and Zamanabad basins (Fig. 7), the sense of throw in 1988 was down to the west, in agreement with the seismology and SAR, and with the formation of the basins themselves.

More problematic than the sense of throw is that some ruptures observed in 1998 and 1981 had an apparent *reverse* sense of displacement, on steeply east- or west-dipping faults. The significance of this apparent shortening is not clear and unambiguous exposures of the faults in cross-section were rare. In 1998 only two were visible, exposed for a depth of about a metre at the base of a steep scarp, dipping west at 65° and 78° between Hashtadan and Fandoqa. At these two places the local strike of the ruptures was 10° – 20° anticlockwise from the overall strike of 156° , and the shortening may be a localized restraining-bend effect. In 1981 the vertical offsets were generally smaller (Fig. 8), but clearly involved shortening in some places (see photos in Figs 11 and 12 of Berberian *et al.* 1984). It is difficult to know how to interpret these observations. The 1981 fractures in particular were often very complex, involving distributed fissuring and cracking over a relatively wide zone, and normal faults were also seen, sometimes associated with thrusts (Fig. 14 in Berberian *et al.* 1984). Some of the apparent shortening may have been related to minor irregularities in the trend of the fault zone or to local topographic effects steepening faults at shallow depth adjacent to older scarps. These surface observations in 1981 greatly influenced our tectonic interpretation in Berberian *et al.* (1984), causing us to suggest that the Gowk valley was bounded by outward-dipping reverse faults (Fig. 23),

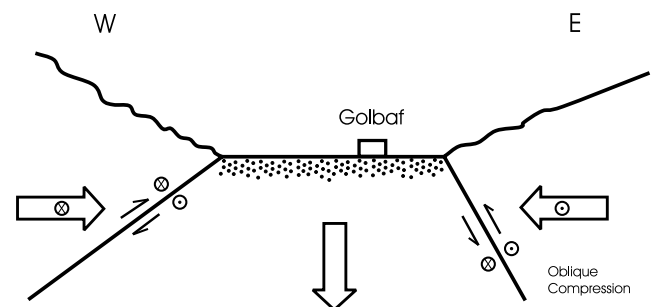


Figure 23. Cartoon cross-section from Berberian *et al.* (1984) to illustrate their suggestion that the depressions in the Gowk valley were formed by subsidence in the footwalls of two opposing thrusts. This suggestion is not compatible with the normal faulting component inferred from seismological and SAR data after the 1998 Fandoqa earthquake.

but it is difficult to reconcile that interpretation with the much better SAR and seismology data now available after the 1998 Fandoqa earthquake.

Why should the Gowk fault system be so complicated? Kinematically, there is no difficulty with local extension in the Gowk Valley occurring in a region of overall shortening, provided that extension is matched by shortening somewhere else, presumably on the Shahdad thrusts. The extension can be a necessary consequence of the overall fault geometry, as it is in Fig. 22(g), and we suspect that it is enhanced in this case by the high topographic contrast between the Dasht-e-Lut and both the Kerman plateau and the Gowk valley, providing a buoyancy force pushing outwards from the high plateau. If a decoupling horizon of lake beds or evaporites exists at shallow depth beneath the Shahdad thrusts, it is easy to see how the edge of the plateau can have a tendency to collapse.

Finally, it is clear that whatever the overall fault geometry is beneath the Gowk valley, it must be unstable and should be evolving. For this reason structural complexities where the faults meet at depth might well provide a barrier to rupture propagation, perhaps making more plausible the suggestion that the 1981 earthquakes ruptured deeper parts of the fault system which later moved at shallower depths in 1989 and 1998. If the faults were continuous and simple between the surface and the base of the seismogenic layer, it is difficult to see why rupture should be halted at depth. On the basis of our preferred interpretations for the 1981 Sirch earthquake (a deep low-angle oblique thrust) and the 1981 Golbaf earthquake (a deep, but steeper, oblique reverse fault) it is even possible that a geometry comparable to Fig. 22(g) occurs north of Zamanabad and one similar to that in Fig. 22(f) occurs south of Zamanabad. This would at least account for the apparent significance of Zamanabad as a place where lateral rupture propagation frequently appears to halt.

10 DISCUSSION

One motivation for this study was the apparent re-rupture of the Gowk fault at the surface in repeated earthquakes after only a short time interval of 17 years (1981–1998). In one place, the surface offsets were much larger in an earthquake of M_w 6.6 in 1998 than they were for an earthquake of M_w 7.1 in 1981 whose moment was 10 times greater. However, there is apparently more to the story than that. It now seems likely that the fault that ruptured in 1998 was not the one on which the main rupture occurred in 1981, although it was reactivated at the surface in 1981 to some extent. We suspect that the 1981 ruptures occurred on deeper parts of a complicated fault system that later broke at shallower depths in March 1998 (and possibly in smaller earthquakes in November 1989 and November 1998 as well). Even with the information available from seismology, SAR interferometry, geomorphology and detailed mapping of the surface ruptures by the same people after each earthquake, it is difficult to understand what happened in these earthquakes and much of our interpretation is speculative. This experience is a caution against simplistic interpretations of palaeoseismological (trenching) investigations and accounts of historical earthquakes, where the amplitude of surface offsets may not be a reliable guide to the magnitude of the earthquake and repeated damage in the same place may not indicate that the same fault moved twice in the same way.

Even without such caution, definitive examples of earthquakes that repeat within a short time interval on apparently the same fault are rare. They are interesting because of their implications for the nature of stress build-up, release and triggering during the earthquake cycle. We are aware of three other examples, also on strike-slip faults. One is in eastern Iran, where parts of the Abiz fault, which ruptured over its entire length of 125 km in 1997 (M_w 7.2), had ruptured at the surface in smaller earthquakes in 1979 (M_w 6.6 and 5.9) and possibly in 1936 (M_s 6.0) as well (Berberian *et al.* 1999). A second is in California, where a section of the Imperial fault that ruptured in 1940 (M_s 7.1) ruptured again in 1979 (M_s 6.6) (Sharp *et al.* 1982). Finally, in Turkey an overlap occurred in the surface rupture zones of two earthquakes on the North Anatolian fault in 1957 (M_s 7.0) and 1967 (M_s 7.1) (Ambraseys & Zatopek 1969; Barka 1996).

The Gowk fault system is also a modern active example of how oblique regional convergence is achieved by faulting. To some extent the strike-slip and thrust components are spatially separated, but this occurs in a manner far more complicated than it does in many island arcs. Even though our understanding of the fault configuration on the Gowk system is imperfect, it is clear that the present geometry is unstable and must evolve with time. In general this is probably the reason why spatially distributed and complex patterns of faulting, often called ‘flower structures’, develop in such places. Other modern examples of such structures that have moved in earthquakes are known, one of the best being from the great 1957 Gobi-Altai earthquake ($M_w \sim 8$) in Mongolia (Kurushin *et al.* 1997). That too produced surface ruptures on subparallel strike-slip and thrust faults, and the evolution of geomorphology and drainage provides some insight into how those structures evolve with time (Bayasgalan *et al.* 1999). The Gowk system has the added complication of an extensional component on the strike-slip system, which may be related to the great topographic contrast (~ 2000 m) between the Kerman plateau and the Dasht-e-Lut. In this example too, the parallel set of ridges that make up the Shahdad thrust system, and the drainage patterns associated with both those ridges and the Gowk valley, give insights into how the structures evolve with time, which will be reported elsewhere.

11 CONCLUSIONS

An excellent set of observations from surface faulting, seismic waveforms, SAR interferometry and surface geomorphology was available after the 1998 March 14 Fandoqa earthquake on the Gowk fault system of central Iran. It is nonetheless difficult to produce an account of what happened that is consistent with all the observations. Seismology and SAR interferometry give a simple picture of oblique right-lateral and normal slip averaging about 1.3 m on a fault dipping west, yet some of the most dramatic surface ruptures were associated with faulting down-thrown to the east. SAR interferometry indicates that a nearby thrust dipping at 6° moved about 8 cm in a time interval and position that makes it likely that its motion was triggered by rupture on the main strike-slip fault. Earlier earthquakes on the Gowk fault in 1981, which also produced relatively minor ruptures at the surface, probably occurred principally on different, deeper parts of the same fault system. The overall picture is one in which regional oblique right-lateral and convergent motion is achieved by a complex system of strike-slip, normal and thrust faulting, with the normal component related

either to a change in dip of the thrust faulting at depth (possibly a 'ramp-and-flat' configuration) or to a large topographic contrast across the fault system, or to both. Although details of how the fault system accommodates regional motions remain speculative, it is clear that no geometry that is consistent with the available evidence is also stable for large finite motions. The system must evolve with time, which is probably the main reason that the distributed geological features known as flower structures develop in such places.

ACKNOWLEDGMENTS

We thank the Geological Survey of Iran, and particularly its Director, Mr M. T. Korehi, for supporting all the field-work aspects of this work, including international travel for MB. Mr R. Rovani kindly arranged logistics in Kerman. We thank C. Johnson of Najarian Associates for drafting maps, and Amerada Hess, BP and King's College for supporting MT in Cambridge. RW is supported by a NERC studentship. The SAR interferometry work was supported by NERC grant GR3/11737 and some of it was carried out at the Jet Propulsion Laboratory, California Institute of Technology, under a contract with the National Aeronautics and Space Administration. ERS SAR images were provided by ESA under project A03-213. Dr T. O. Najarian kindly helped with publication costs. We thank R. Norris and D. Hatzfeld for careful reviews, although we alone are responsible for any remaining errors or misconceptions. Cambridge Earth Sciences contribution 6317.

REFERENCES

- Ambraseys, N.N. & Melville, C.P., 1982. *A History of Persian Earthquakes*, Cambridge University Press, New York.
- Ambraseys, N.N. & Zatopek, A., 1969. The Mudurnu valley earthquake of July 22, 1967, *Bull. seism. Soc. Am.*, **59**, 521–589.
- Barka, A., 1996. Slip distribution along the North Anatolian Fault associated with the large earthquakes of the period 1939 to 1967, *Bull. seism. Soc. Am.*, **86**, 1238–1254.
- Bayasgalan, A., Jackson, J., Ritz, J-F. & Carretier, S., 1999. 'Forebergs' flower structures and the development of large intracontinental strike-slip faults: the Gurvan Bogd fault system in Mongolia, *J. struct. Geol.*, **21**, 1285–1302.
- Berberian, M., 1981. Active faulting and tectonics of Iran in *Zagros-Hindu Kush-Himalaya Geodynamic Evolution*, *Am. geophys. Un., Geodyn. Ser.*, Vol. 3, pp. 33–69 eds Gupta, H.K. & Delany, F.M., AGU, Washington.
- Berberian, M. & Qorashi, M., 1994. Coseismic fault-related folding during the south Golbaf earthquake of November 20, 1989, in southeast Iran, *Geology*, **22**, 531–534.
- Berberian, M. & Yeats, R.S., 1999. Patterns of historical earthquakes rupture in the Iranian plateau, *Bull. seism. Soc. Am.*, **89**, 120–139.
- Berberian, M., Jackson, J.A., Qorashi, M. & Kadjar, M.H., 1984. Field and teleseismic observations of the 1981 Golbaf-Sirch earthquakes in SE Iran, *Geophys. J. R. astr. Soc.*, **77**, 809–838.
- Berberian, M., Jackson, J.A., Qorashi, M., Khatib, M.M., Priestley, K., Talebian, M., Ghafari-Ashtiani, M., 1999. The 1997 May 10 Zirkuh (Qa'enat) earthquake (M_w 7.2): faulting along the Sistan suture zone of eastern Iran, *Geophys. J. Int.*, **136**, 671–694.
- Berberian, M., Jackson, J.A., Qorashi, M., Talebian, M., Khatib, M. & Priestley, K., 2000. The 1994 Sefidabeh earthquakes in eastern Iran: blind thrusting and bedding-plane slip on a growing anticline, and active tectonics of the Sistan suture zone, *Geophys. J. Int.*, **142**, 283–299.
- Clarke, P.J., Paradissis, D., Briole, P., England, P.C., Parsons, B.E., Billiris, H., Veis, G. & Ruegg, J-C., 1997. Geodetic inversion of the 13 May 1995 Kozani-Grevena (Greece) earthquake, *Geophys. Res. Lett.*, **24**, 707–710.
- Engdahl, E.R., van der Hilst, R. & Buland, R., 1998. Global teleseismic earthquake relocation with improved travel times and procedures for depth determination, *Bull. seism. Soc. Am.*, **88**, 722–743.
- Fitch, T.J., 1972. Plate convergence, transcurrent faults and internal deformation adjacent to southeast Asia and the western Pacific, *J. geophys. Res.*, **77** 4432–4460.
- Jackson, J.A. & McKenzie, D.P., 1984. Active tectonics of the Alpine-Himalayan belt between western Turkey and Pakistan, *Geophys. J. R. astr. Soc.*, **77**, 185–264.
- Jackson, J.A., Haines, A.J. & Holt, W.E., 1995. The accommodation of Arabia–Eurasia Plate Convergence in Iran, *J. geophys. Res.*, **100**, 15 205–15 219.
- Kurushin, R.A. *et al.*, 1997. The surface rupture of the 1957 Gobi-Altay, Mongolia, earthquake, *Geol. Soc. Am. Spec. Paper*, **320**, 1–143.
- Massonnet, D., Rossi, M., Carmona, C., Adragna, F., Peltzer, G., Fiegl, K. & Rabaute, T., 1993. The displacement field of the Landers earthquake mapped by radar interferometry, *Nature*, **364**, 138–142.
- Massonnet, D. & Fiegl, K.L., 1998. Radar interferometry and its application to changes in the Earth's surface, *Rev. Geophys.*, **36**, 441–500.
- McCaffrey, R., 1992. Oblique plate convergence, slip vectors, and forearc deformation, *J. geophys. Res.*, **97**, 8905–8915.
- McCaffrey, R. & Abers, G., 1988. SYN3: a program for inversion of teleseismic body waveforms on microcomputers, *Air Force Geophys Lab. Tech. rept*, AFGL-TR-88-0099, Hanscomb Air Force Base, MA.
- McCaffrey, R. & Nabelek, J., 1987. Earthquakes, gravity and the origin of the Bali basin: an example of a nascent continental fold-and-thrust belt, *J. geophys. Res.*, **92**, 441–460.
- McCaffrey, R., Zwick, P. & Abers, G., 1991. SYN4 Program, *IASPEI Software Library*, **3**, 81–166.
- Mirza'i-Alavicheh, H. & Farzanegan, E., 1998. The 23 Esfand 1376 Golbaf, Kerman, earthquake, *Tazehayeh Sakhteman va Maskan*, **8**, 34–35 (in Persian).
- Molnar, P. & Lyon-Caen, H., 1989. Fault plane solutions of earthquakes and active tectonics of the Tibetan Plateau and its margin, *Geophys. J. Int.*, **99**, 123–153.
- Nabelek, J., 1984. Determination of earthquake source parameters from inversion of body waves, *PhD thesis*, MIT, Cambridge, MA.
- Okada, Y., 1985. Surface deformation due to shear and tensile faults in a half space, *Bull. seism. Soc. Am.*, **75**, 1135–1154.
- Scholz, C.H., Aviles, C. & Wesnousky, S., 1986. Scaling differences between large intraplate and interplate earthquakes, *Bull. seism. Soc. Am.*, **76**, 65–70.
- Sharp, R.V., *et al.*, 1982. Surface faulting in the central Imperial Valley, in: *The Imperial Valley, California, Earthquake of October 15, 1979*. *USGS Prof. Paper*, **1254**, 119–143.
- Taymaz, T., Jackson, J. & McKenzie, D., 1991. Active tectonics of the north and central Aegean Sea, *Geophys. J. Int.*, **106**, 433–490.
- Wright, T.J., Parsons, B.E., Jackson, J.A., Haynes, M., Fielding, E.J., England, P.C. & Clarke, P.J., 1999. Source parameters of the 1 October 1995 Dinar (Turkey) earthquake from SAR interferometry and seismic bodywave modelling, *Earth planet. Sci. Lett.*, **172**, 23–37.
- Zwick, P., McCaffrey, R. & Abers, G., 1994. MT5 Program, *IASPEI Software Library*, **4**.